

UK UNCLASSIFIED - US FOR OFFICIAL USE ONLY

Evaluation of Modern HF Ray Tracing [Final Report] - UC

DERA/CIS/CIS1/CR990854

Copy 1 of 10

Cover + x + 48 pages

November 1999

DISTRIBUTION STATEMENT A

Approved for Public Release
Distribution Unlimited

Neil Rogers

20010606 080

This document is subject to
the release conditions printed
on the reverse of this page

DERA

DERA is an Agency of the UK Ministry of Defence

UK UNCLASSIFIED - US FOR OFFICIAL USE ONLY

AQ FOI-09-1607

Customer Information

Customer Reference Number	
Project Title	Evaluation of Modern HF Ray Tracing
Company Name	University of Bath, UK.
Customer Contact	Prof. P. Watson
Contract Number	CSM 7153
Milestone Number	002
Date Due	30/11/1999

This Document was produced by DERA for the University of Bath, UK. under Order/Contract reference CSM 7153

Copying and use of the document is restricted to that set out in the above Order/Contract and the document may not otherwise be used or disseminated without written consent of DERA.

© Crown copyright 1999 Defence Evaluation and Research Agency UK


Approval for wider use of releases must be sought from:

Intellectual Property Department, Defence Evaluation and Research Agency,
DERA Farnborough, Farnborough, Hampshire GU14 0LX

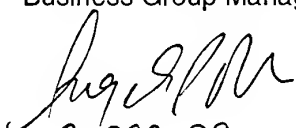
DERA/CIS/CIS1/CR990854

Authorisation

Prepared by Neil Rogers
Title Scientist

Signature 
Date 30 - Nov - 99
Location D714, DERA Malvern

Authorised by Angela Noble
Title Business Group Manager

Signature 
Date 2 - Dec - 99

Principal authors

Name Neil Rogers
Appointment Scientist
Location D714, DERA Malvern

Name Prof. P.S. Cannon
Appointment Head, Radio Science and Propagation Group
Location D705, DERA Malvern

Record of changes

Issue	Date	Detail of Changes
1.0	30/11/99	First Issue.

Abstract

In this report the accuracy of a novel segmented method for analytic ray tracing (SMART) developed at DERA is reported alongside numerical and virtual mirror ray tracing techniques. A description is given of a homing technique for the synthesis of oblique incidence (OI) ionograms by means of SMART ray tracing. Synthetic OI ionograms have been compared against measured OI ionograms on six UK paths. By scaling key parameters from each ionogram (synthetic vs. measured) the accuracies of four climatological ionospheric models, tomographic images and the Parameterised Real-time Ionospheric Specification Model (PRISM) are described.

(UC)

Executive summary

This is the final report of the project entitled "Evaluation of Modern HF Ray Tracing". The report reviews some of the ray tracing validation studies and ionospheric tomography experiments already conducted by DERA. Further research including validation of ITU Recommendation 533-3 [ITU, 1992] and the PRISM model is also described.

The large number of ray-tracing techniques currently available provides a diverse range of options for beyond line of sight systems. A numerical ray-tracing method together with an accurately specified ionospheric model provides a high level of accuracy but may be time consuming in execution. However, analytical techniques have been developed which can provide a tenfold improvement in execution speed whilst retaining ground range and power loss accuracies to within 5% of the numerical values.

The accuracy of a novel segmented method for analytical ray tracing (SMART) is described in this report with reference to the results of a numerical ray-tracing program. The comparative speed and accuracy of these techniques is presented and the benefits and limitations of each method are discussed. Tests of the models were performed at two different HF frequencies in regions of large and small horizontal ionospheric electron density gradients (low-latitude and mid-latitude respectively).

A commonly implemented, fast alternative to ray-tracing is the 'virtual mirror' method for ground range determination which involves finding the height of a horizontal, plane mirror that would simulate the effect of ionospheric refraction at the mid-point of a Tx-Rx path and determining the elevation angle as a geometrical function of the ground range. One such method incorporated into ITU Recommendation 533-3 [ITU, 1992] is described here and the results compared with those obtained using both a numerical and an analytical raytrace through a DUD profile [Dudeney, 1978] fitted to the ITU model ionospheric parameters. Ground range differences in excess of 500km are observed for 5MHz rays at elevation angles within a few degrees of the transition between E and F-mode propagation.

A new homing technique has been used to synthesise oblique incidence (OI) ionograms over six UK paths for which real OI ionograms have been obtained. Synthetic OI ionograms were produced by means of ray tracing through electron density models generated from climatological models (FAIM, PIM, and IRI-95), a real-time updated specification model (PRISM) and tomographic images. Six points were scaled from each synthesised OI ionogram and these were compared against values from the corresponding real ionogram and the differences used as a measure of model accuracy. Parameters predicted from the ITU Rec. 533 method were also compared with the IRIS-scaled measurements.

Synthetic OI ionograms produced by ray tracing through either the tomographic images or the climatological models generally underestimated the average

maximum usable frequency (MUF) of the E trace (MUF(E)). The best climatological model (IRI-95) underestimated MUF(E) by only 1.4% compared with at least 5.3% for the best tomographic method.

In contrast, tomography generally overestimated MUF(F2) but in this case tomography performed better than the climatological models. The best tomographic method predicted a mean 0.8% overestimate compared with 3.3% for the best climatological method. Climatology also showed larger rms errors than tomography for both MUF(E) and MUF(F2).

When no ionosonde was used to provide *a priori* information in the tomographic reconstruction, the average underestimate of MUF(E) increased from 5.3% to 20.2% and the average MUF(F2) overestimate increased from 0.8% to 3.3%. The use of more than one ionosonde did not reduce further the errors associated with the tomographic images.

The minimum delay of the E trace ($m'd(E)$) (a measure of the height of the E layer) was better represented by tomography (0.1% mean underestimate) than climatology (at least 2.1% mean error). However, tomography consistently underestimated the minimum delay of the F trace (by at least 2.8%) unlike the climatological models (mean underestimate 0.5%).

Using real-time updating information from the Chilton and Lerwick ionosondes, the PRISM model produced smaller errors than the PIM model. The average overestimates reduced from -12.9% to 0.5% for MUF(E), 16.6% to 5.4% for MUF(F2), 2.1% to -1.8% for the minimum delay of the E trace, $m'd(E)$ and -0.8% to 0.2% for $m'd(F(F1))$, the minimum delay of the F (or F1) trace.

ITU Recommendation 533 produced very large errors in $m'd(F(F1))$ (average 21.6% overestimated) but errors in other parameters were comparable with other models.

Considerable errors in the delay of the entire F trace were observed in many synthetic ionograms when F1 traces were observed on the measured ionograms. A faithful reproduction of the shape of the divided F trace was only achieved by ray tracing through tomographic images incorporating a full electron density profile from an ionosonde. The large error in F-region trace delay would lead to similarly large errors in the ground range of propagating HF rays. It is therefore recommended that the representation of the F1 region in real-time ionospheric models be given careful consideration.

List of contents

Authorisation	iii
Record of changes	iv
Abstract	v
Executive summary	vi
List of contents	viii
1 Introduction	1
1.1 Contractual Matters	1
1.2 Purpose	1
1.3 Project Objectives	1
1.4 Project Organisation	1
1.5 Scope of the Report	1
1.6 Structure of the Report	2
2 Background	3
2.1 Analytical Ray Tracing Techniques	3
2.2 Numerical Ray Tracing Techniques	5
2.3 Ionospheric Electron Density Models	5
2.4 The Virtual Mirror Technique for Ground Range Determination	6
2.5 The IRIS Oblique Sounder Network	7
2.6 Tomographic Imaging of the Ionosphere	8
3 Validation of ray tracing algorithms	10
3.1 Methodology	10
3.2 Results	10
4 Integration of PIM/PRISM with SMART	16
4.1 Implementation	16
4.2 Suggestions for Future Research	16
5 Synthesis of Oblique Ionograms by Ray Tracing	20
5.1 Introduction	20
6 Validation of ionospheric models using IRIS Ionograms	24
6.1 Introduction	24

6.2	Methodology	24
6.3	Results	26
6.4	Case Study: Synthetic and measured ionograms on the Cove Malvern path – 6 th April 1998, 1516UT.	30
7	Conclusions	36
8	Recommendations for Further Work	37
8.1	Validation and Development of the PRISM model	37
8.2	Importance of the F1 layer	37
9	Acknowledgements	38
10	References	39
11	List of Symbols	41
12	List of abbreviations	42
A	Flow diagram for homing ray trace algorithm	43
	Distribution list	47
	Report documentation page	49

This page is intentionally blank

1 Introduction

1.1 Contractual Matters

- 1.1.1 This report has been issued by DERA for the Department of Electronic and Electrical Engineering, University of Bath under contract CSM/7153 ("Evaluation of Modern HF Ray Tracing"). It constitutes the 1999 deliverable (final report) as described in the proposal.

1.2 Purpose

- 1.2.1 This report summarises research evaluating the accuracy of ionospheric models and ray tracing techniques.

1.3 Project Objectives

- 1.3.1 This project was designed to test and validate modern, physically based models such as the Parameterised Ionospheric Model (PIM) [Daniell *et al.*, 1995], the Parameterised Real-time Ionospheric Specification Model (PRISM) [Daniell, 1991], together with ray tracing algorithms such as the Segmented Method for Analytical Ray Tracing (SMART) [Norman and Cannon, 1997, 1999; Rogers, 1998] and alternative techniques such as 'virtual mirror' algorithms.
- 1.3.2 Recently developed HF analytical ray tracing techniques, and methods to couple these with ionospheric models, were to be assessed and validated.
- 1.3.3 In particular, the proposed activities included
1. Integration of PIM/PRISM with the DERA ray tracing algorithm called SMART (the Segmented Method for Analytical Ray Tracing).
 2. Initial tests, regarding accuracy, with reference to numerical ray tracing.
 3. Development of algorithms to synthesise oblique ionograms using SMART and PIM/PRISM.
 4. Development of a similar synthesis using a monthly median approach with virtual mirror ray tracing, and comparison of results with the SMART/PIM technique.
 5. Comparison of all synthesised ionograms with those from the UK oblique ionosonde network.

1.4 Project Organisation

- 1.4.1 All model and ray tracing testing was performed at DERA. The PRISM model was supplied to DERA by the US Air Force (Space Command) in November 1999 under Project Arrangement No. US-UK-AF-003 (The Effects of the Ionosphere on C³I Systems) – a project under the US-UK Technology Research and Development Project Memorandum of Understanding.

1.5 Scope of the Report

- 1.5.1 This report describes work performed under the contract together with some background work carried out previously. This includes descriptions of ray tracing techniques and

ionospheric models, a homing algorithm used for synthetic oblique incidence ionogram generation and various tests of the ray tracing techniques and ionospheric models.

1.6 Structure of the Report

- 1.6.1 Section 2 provides a background to the ray tracing techniques and ionospheric electron density models used in this study. The UK oblique sounder and ionospheric tomographic imaging networks used in this study are introduced. In Section 3, analytical and 'virtual mirror' ray tracing techniques are compared against numerical ray tracing techniques to provide an indication of the accuracy of each technique.
- 1.6.2 Section 4 describes how the SMART analytical ray tracing software has been incorporated into the HF Electromagnetic Environment Management System (HF-EEMS [Shukla *et al.*, 1997]) along with the PIM model. Examples of the output from the combined system are presented and recommendations for future developments are made.
- 1.6.3 In Section 5 the homing algorithm of the SMART analytical ray tracing software is described in detail. This homing algorithm is used to produce synthetic oblique incidence (OI) ionograms by ray tracing through ionospheric electron density models. Section 6 analyses the accuracy of ionospheric and propagation models by comparing synthetic OI ionograms with ionograms recorded by the UK IRIS oblique sounder network. A case study is also presented to highlight where accuracy improvements may be made.
- 1.6.4 Finally Sections 7 and 8 present some conclusions and recommendations for future work.

2 Background

2.1 Analytical Ray Tracing Techniques

- 2.1.1 An extensive and diverse range of ray tracing methods have been developed over recent years to address the need for quick and reliable determination of the path of HF signals through the ionosphere. These range from simple, geometrical methods based upon an estimate of the 'mirror' height of reflection, to a series of full numerical solutions of the ray equations [*Haselgrove*, 1955] at regular intervals along the projected ray path. Virtual mirror techniques are often employed in frequency coverage prediction programs such as ITU Recommendation 533 [*ITU*, 1992], but these only specify the ionosphere at single 'control' points along the great circle path (for example at the mid-point). For the purposes of ray tracing, many researchers have attempted to recreate the vertical profile of electron density by fitting analytical functions at these control points and then applying a numerical technique to determine the ray path ([*Bradley and Dudeney*, 1973; *Dudeney*, 1978; *Rawer*, 1981; *Booker*, 1977]). This approach fails to take account of any horizontal structure of the ionosphere (such as tilts and troughs) and consequently are only applicable to the relatively unstructured mid-latitude ionospheric regions.
- 2.1.2 A computationally efficient approach to ray tracing has been developed which involves approximating the electron density profile (EDP) with mathematical functions for which the exact solutions to the ray equation may be obtained. It has long been known that the ray equation has exact, analytical solutions if the electron density varies with height above a flat earth as a perfect parabola [*Budden*, 1961]. *Croft and Hoogasian* [1968] have shown that with minor adjustments to this electron density profile, exact solutions of the ground range, group path, phase path and apogee height are calculable for oblique paths over a spherical earth in the absence of a magnetic field. This modified profile is called a Quasi-Parabolic (QP) profile.
- 2.1.3 A number of implementations of the QP method are discussed in *Rogers et al.* [1998]. In the simplest implementation, the QP profile is applied uniformly to the whole ionosphere. Various methods have been attempted to model simple, uniform tilts in the ionosphere by displacing the centre of the spherically stratified ionosphere from the centre of the Earth [*Folkestad*, 1968; *Platt and Cannon*, 1994; *Norman et al.*, 1995].
- 2.1.4 In order to model complex horizontal gradients such as troughs and localised enhancements, an alternative method has been developed at DERA and is called SMART (Segmented Method for Analytical Ray Tracing) [*Norman and Cannon*, 1997; *Norman and Cannon*, 1999; *Rogers*, 1998]. In this approach, the EDP is determined at the point of entry of the ray into the ionosphere, and a series of smoothly attached QP segments are fitted to the profile using the method of least squares. As many QP segments are used as are required to fit the QP to the EDP to within a pre-set error tolerance. This process is illustrated in Figure 2-1. The analytical ray parameters (ground range, group path, etc.) are determined for each successive QP segment until the total ground range within the ionosphere exceeds a limiting value. At this point, the EDP is re-determined (e.g. from a model) and a new set of QP segments fitted. The effective launch elevation angle for the new ionospheric sector is determined using a continuity equation (similar to Snell's law). The ray tracing then proceeds as for the initial ionospheric sector until the ray leaves the ionosphere.

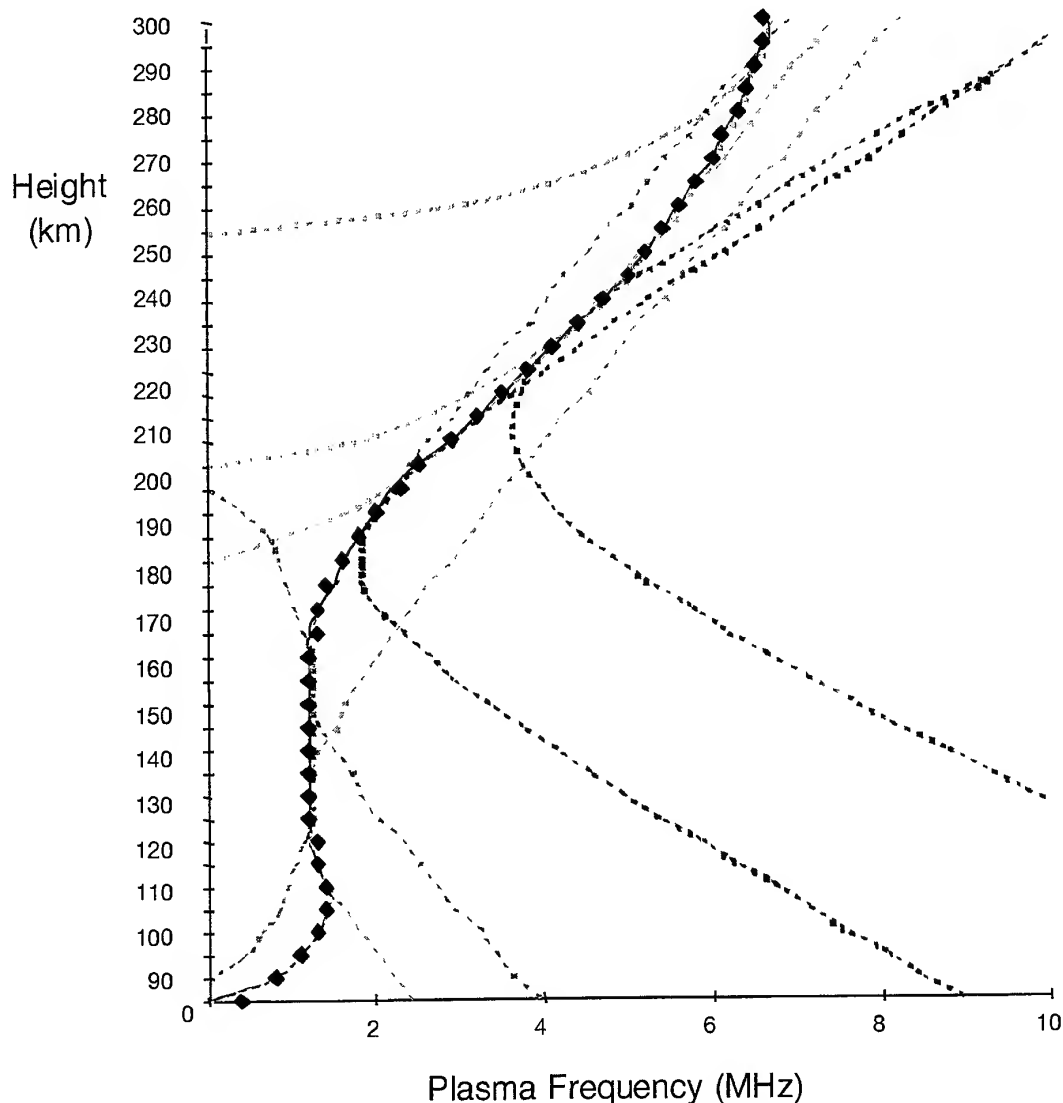


Figure 2-1: Multiple quasi-parabolic (QP) segments (dashed curves) are fitted to the ionospheric profile (diamonds) by the method of least squares. Each QP segment is smoothly attached to adjacent segments. Note that plasma frequency is proportional to the square-root of the electron density.

2.1.5 Rogers *et al.* [1998] performed a detailed evaluation of a range of analytical and numerical ray tracing techniques. These authors concluded that 10-100 fold computational speed improvements could be obtained by employing an analytical ray tracing technique as opposed to a full numerical technique. Where a system is required to 'home-in' to a transmitter, a large number of traces is required and the slow speed of the numerical technique could hinder real-time operations. Rogers *et al.* [1998] also found that the SMART method gave ground range precision to within 5% of the numerically determined values. In addition, the SMART method could accurately ray-trace through ionospheric models incorporating complex horizontal electron density gradients such as those observed at high latitudes and in the equatorial zones.

2.2 Numerical Ray Tracing Techniques

- 2.2.1 Ray tracing through an ionosphere containing complex gradients of electron density is modelled most accurately using a numerical integration of the coupled Haselgrove equations. These six differential equations, representing the ionospheric refractive index and its spatial derivatives, are integrated numerically (unless some analytically soluble ionospheric model profile is applied) in a stepwise manner, continually adjusting the group path step size to ensure the accuracy is kept within pre-defined tolerances. This iterative, numerical approach is an accurate but time consuming method that is often inappropriate for many real-time or near real-time applications.
- 2.2.2 The numerical ray tracing computer program used in this study is a development of the Jones and Stephenson program [Jones, 1968; Jones and Stephenson, 1975] and is called HIRT - the Homing-In Ray Tracing program [Norman *et al.*, 1994]. The program solves the coupled Haselgrove equations using a fourth-order Runge-Kutta interpolation to initiate a fourth-order Adams-Moulton predictor-corrector method that iteratively adjusts the step size at each stage in the numerical integration. The program calculates the ground range, apogee height, phase path and group path for each ray. Phase path is defined as the time taken for a surface of constant phase to travel between the transmitter and receiver multiplied by the speed of radiowaves in free space, c . The group path is defined as c multiplied by the time delay between the launch of a wavepacket at the transmitter and its reception at the receiver. A 'variational ray' technique is also employed to calculate the divergent power loss due to radial divergence (free space loss) and any ionospheric focusing or defocusing over each ray path.
- 2.2.3 The refractive index term involving the frequency of collisions between electrons and neutrals has been neglected in this study since analytical ray tracing methods cannot model this process. Thus, the power loss calculations in this study do not consider the absorption that occurs in the lower (D region) ionosphere. This absorption is caused by the radiowave imparting energy to the free electrons, which then collide with neutral molecules such that the radiowave energy is lost to the neutral atmosphere as heat.

2.3 Ionospheric Electron Density Models

- 2.3.1 Of course, there is little advantage in operating a highly accurate ray-tracing tool when the associated benefits are overwhelmed by the inaccuracies of the ionospheric model. The ionospheric distribution of electron density is directly related to the refractive index and must therefore be accurately specified. Isolated measurements of the electron density structure may be obtained from ionospheric sounders, or by tomographic imaging, but for large areas of the globe, an ionospheric model is required.
- 2.3.2 The Fully Analytical Ionospheric Model (FAIM) [Anderson *et al.*, 1989] is a global, parameterised model based on low latitude physical models of the ionosphere. It is particularly appropriate for low and mid-latitude applications. FAIM uses the formalism of the Chiu model [Chiu, 1975], with the coefficients fitted to profiles of the Semi-empirical Low-latitude Ionospheric Model, SLIM [Anderson *et al.*, 1987]. The model calculates the total electron density (and constituent ion densities) given input parameters of latitude, longitude, height, month, F10.7 and local time. A major advantage of the FAIM model is its speed of execution.
- 2.3.3 The Parameterized Ionospheric Model (PIM) [Daniell *et al.*, 1995] is a global climatological model incorporating four physical models of the ionosphere - F layer models of the low and mid-latitude regions, a combined low and mid-latitude E layer

model and a high-latitude E and F layer model. All four models use the ISIS 86 neutral atmosphere model [Hedin, 1987]. PIM is parameterised by the latitude, longitude, year, day number, time of day, level of solar and geophysical activity (sunspot number and K_p) and orientation of the interplanetary magnetic field (B_y and B_z). The model generates vertical profiles of the electron density from these parameters and the following "anchor points" are derived from these profiles:-

- foF2 the F2 layer critical plasma frequency (or vertical penetration frequency),
- hmF2 the height of maximum electron density in the F2 region,
- foE the E layer critical plasma frequency,
- hmE the height of the maximum electron density in the E region.

Note that F1 layer parameters are not provided in the version of PIM used in this study (Version 1.6).

- 2.3.4 PIM incorporates the high latitude Utah State University model [Schunk, 1988] making it a truly global model (unlike FAIM). PIM forms the core of a recently developed real-time ionospheric specification system, PRISM (Parameterised Real-time Ionospheric Specification Model) [Daniell, 1991].

2.4 The Virtual Mirror Technique for Ground Range Determination

- 2.4.1 The virtual mirror technique is a straightforward alternative to the conventional ray-tracing techniques described above where the ground range is required as a function of the elevation angle of the ray. This geometrical technique requires an estimation of the height of a plane mirror reflector that would emulate the refractive deviation of the ray path in the ionosphere. This mirror height may be estimated from ionospheric parameters evaluated at the path mid-point which is itself a function of the ground range. Thus this process of ground range determination is inherently iterative. No correction is made for the magnetic field and horizontal gradients in the ionospheric electron density are not considered.
- 2.4.2 In this study, the reflection height is determined at the path midpoint for a range of single hop path lengths using the semi-empirical techniques described in ITU Recommendation 533 [ITU, 1992]. The elevation angle is then calculated geometrically as a function of ground range. In a practical system this function could be inverted to provide ground range estimation as a function of the elevation angle.
- 2.4.3 The virtual mirror technique may also be implemented using vertical incidence (VI) ionograms to estimate the virtual heights of reflection downrange. If a signal of frequency f arrives at an elevation angle of β the virtual height, h' , is determined from the VI ionogram at the 'equivalent vertical incidence frequency' of $f \sin(\beta)$ (for a flat earth). The range to the transmitter (assuming a single hop over flat earth) is then $2h'/\tan(\beta)$.
- 2.4.4 This report presents comparisons for the former virtual mirror technique (using a global model of reflection heights – ITU Rec. 533). The ionogram method is only applicable over short ground ranges (about 100 km for E modes, 300 km for F modes) due to the assumption that the ionosphere downrange is identical to that directly overhead. In addition, exact solutions are not available for a curved earth and this leads to errors in the calculation of the equivalent vertical incidence frequency on longer paths. These

errors are particularly significant near any cusp in the ionogram (e.g. between E and F region ionogram traces).

2.5 The IRIS Oblique Sounder Network

2.5.1 The accuracy of ionospheric electron density models has been assessed by ray tracing through them to synthesise oblique ionograms (see Section 5) and then comparing these with real ionograms recorded simultaneously. The latter were obtained from the UK section of the IRIS (Improved Radio Ionospheric Sounder) network. *Arthur et al. [1997]* provide a detailed description of the configuration of IRIS equipment.

2.5.2 The location of transmitters and receivers on the IRIS network are illustrated in Figure 2-2 and listed in Table 1. For reference, the great circle path lengths are provided in Table 2, bearings of the receivers in Table 3, and great circle path midpoints in Table 4.

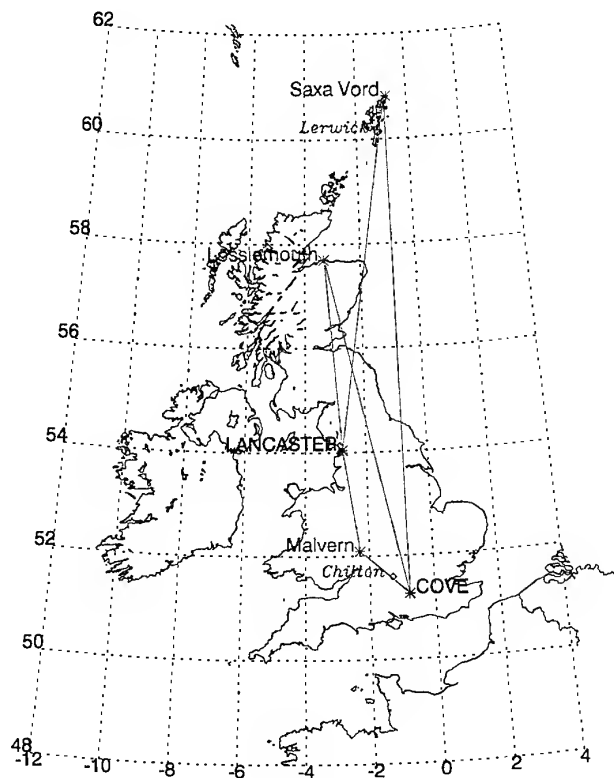


Figure 2-2: The UK IRIS oblique sounder network. Transmitters are labelled in upper case, receivers in lower case, and independent vertical incidence ionosondes in small *Italics*. Great circle propagation paths are also shown.

	Latitude (°N)	Longitude (°E)
Transmitters:		
Cove	51.27	-0.8
Lancaster	54.05	-2.8
Receivers:		
Lossiemouth	57.71	-3.34
Malvern	52.1	-2.3
Saxa Vord	60.83	-0.83

Table 1: Locations of Transmitters and Receivers of the UK IRIS oblique sounder network.

	Lossiemouth	Malvern	Saxa Vord
Cove	712.84	138.58	1062.86
Lancaster	408.29	219.35	762.85

Table 2: Great circle path lengths (km) of the UK IRIS oblique sounder network. Values are calculated assuming a spherical Earth with a radius of 6370.00km.

	Lossiemouth	Malvern	Saxa Vord
Cove	347.69	312.34	359.91
Lancaster	355.49	171.04	8.06

Table 3: Bearing (degrees) of receivers (measured from transmitter locations) in the UK IRIS network.

	Lossiemouth	Malvern	Saxa Vord
Cove	54.40N, -1.97E	51.69N, -1.54E	56.05N, -0.81E
Lancaster	55.88N, -3.06E	53.08N, -2.54E	57.44N, -1.91E

Table 4: Locations of the midpoints of the UK IRIS oblique sounder network great circle paths.

2.5.3 The Rutherford Appleton Laboratory (RAL) operated the IRIS transmitter at Lancaster between 22/12/97 and 6/6/98.

2.5.4 The transmitters and receivers of the IRIS network are synchronised by GPS timing signals. This allows for a measurement of the absolute group delay (time-of-flight) which can then be compared directly with the group delay predictions from the ray tracing.

2.6 Tomographic Imaging of the Ionosphere

2.6.1 A research programme of ionospheric tomographic imaging has been conducted at DERA over the period 1996-1999 in collaboration with the University of Wales, Aberystwyth. Tomographic techniques have produced two-dimensional images of the electron density in the ionosphere along a geographic meridian. The images are reconstructed from projections (or line integrals) of the electron density (known as the Total Electron Content – TEC), measured on a large number of satellite-ground paths that cross the ionosphere at a range of angles. TEC is determined using a “differential Doppler” technique in which the phase difference between two phase-coherent radio signals transmitted from polar orbiting satellites at two widely spaced V/UHF frequencies is measured.

- 2.6.2 The UK tomographic receiver chain is comprised of five receivers extending from Dartmouth (50.3°N, 3.6°W) to Saxa Vord, Shetland Is. (60.8°N, 0.8°W) (see Figure 2-3). Each receiver recorded the phase of 150MHz and 400MHz signals from beacons aboard the Naval Ionospheric Measuring System (NIMS) satellites. Measurements were collated at Aberystwyth and reconstruction algorithms are applied to derive tomographic images.

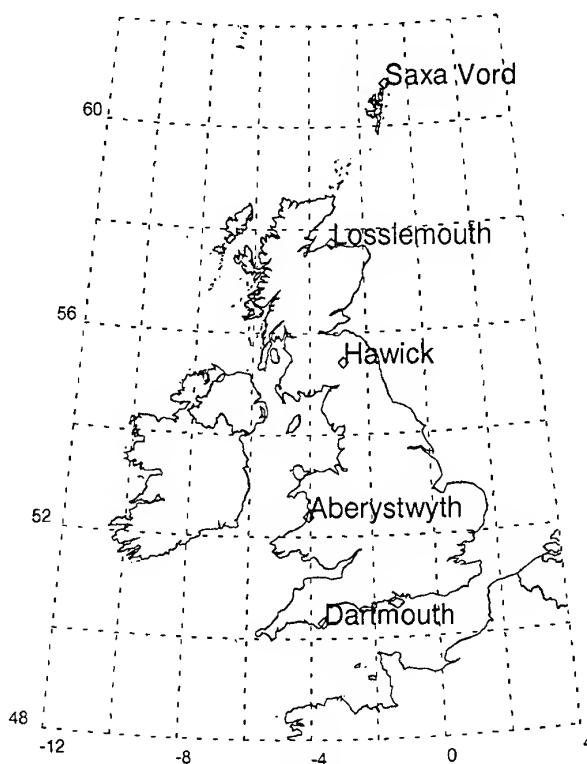


Figure 2-3: Sites of the UK Tomographic receiver chain.

- 2.6.3 Tomographic research at DERA focussed upon improvements to the accuracy of the electron density images, particularly with regard to their vertical structure. Vertical electron density profiles were derived from ionosonde measurements at Chilton (51.6°N, 1.3°W) and Lerwick (60.2°N, 1.2°W) and used to improve the representation of the vertical electron-density profile in the images.
- 2.6.4 The resulting tomographic images show extreme variability of the ionosphere over the UK, with large-scale electron density structures (sometimes associated with the auroral zone) observed at UK latitudes during geomagnetic storms. The tomographic images indicate that the sub-auroral trough in the ionospheric F layer is routinely present over the northern UK at night. With enhanced geomagnetic disturbance a progression of the trough to lower latitudes is observed, and extremely disturbed geomagnetic conditions result in the trough minimum being as far south as northern France.

3 Validation of ray tracing algorithms

3.1 Methodology

- 3.1.1 ITU recommendation 533-3 [ITU, 1992] provides a fast alternative to conventional ray tracing which is used principally for determining broadcast signal coverage in communications applications. This method involves replacing the ionosphere with a horizontal, plane mirror at a height determined from the hop length and a set of ionospheric parameters (f_oF_2 , f_oE , $h'F(F_2)$ and $M(3000)F_2$) obtained from the ITU database which describe the ionospheric profile at a control point on the path. The ITU database contains monthly median values obtained by a world-wide network of about 150 ionosondes during the years 1954 to 1958,
- 3.1.2 For the purposes of comparison, we have constrained the model such that only one-hop paths are considered and the hop length is such that the control point is always at the mid-point of the path. Rec. 533 imposes a maximum single-hop range for F2 modes of 4000km (2000km for E modes) and the minimum elevation angle is 3° .
- 3.1.3 The basic MUF of the 1F2 mode is evaluated first and if this falls below the transmission frequency then the ray for that range is assumed to have penetrated the ionosphere. Secondly the height of reflection for the 1F2 mode is determined as a function of time, location, hop length and sunspot number (R_{12}). The elevation angle corresponding to this height is calculated geometrically. This angle is used in the determination of the E-layer screening frequency. If this frequency exceeds the transmission frequency a 1E mode of propagation is assumed and the elevation angle is determined using an equivalent plane mirror reflection height of 110km.
- 3.1.4 The $M(3000)F_2$ value used in determining F2 region mirror reflection heights is uniquely obtained from the ITU database of ionogram scaled parameters and is unobtainable from an analysis of ionospheric model EDPs. For this reason, a direct comparison between the results of the Rec.533 method and the conventional raytracing methods using the physical models such as FAIM cannot be made. However, a DUD model profile [Dudeney, 1978] can be fitted to parameters from the ITU database. Empirical equations given in [Dudeney, 1974] are used to determine h_mF_2 and y_mF_2 , the peak height and semi-thickness of the F2 region respectively from ITU parameters $h'F(F_2)$, $M(3000)F_2$ and 12-month smoothed sunspot number R_{12} . Thus a comparison of the relative speed and accuracy of the two approaches is made possible. This method of comparison (developed under a previous contract) is discussed in more detail by Rogers *et al.* [1998].

3.2 Results

- 3.2.1 Plots of ground range vs. elevation angle calculated by the SMART, HIRT and ITU techniques are presented in Figure 3-1 to Figure 3-4 for the mid-latitude and low-latitude region at 5 MHz and 14 MHz. Mid-latitude ray traces were performed due south of $55^\circ N$ and low-latitude ray traces were performed south of $32^\circ N$. Note that in the ITU Rec.533 method, the elevation angle is determined as a single-valued function of the ground range whereas the opposite is true for conventional ray-tracing techniques. In the 5 MHz plots (Figure 3-3 and Figure 3-4), Rec533 predicts an E-mode of propagation for elevation angles up to 25° and an F mode for elevation angles above 25° on both paths. The E mode predictions on both paths consistently exceed those obtained using the DUD profile by 50-150 km. F mode ground range predictions converge at the higher

elevation angles (above 45°). It is clear that at the transition between E and F modes of propagation the differences in the two models are considerable, with ground range errors typically of the order of 100 km. The Rec. 533 method effectively ignores those rays which approach the E-mode skip (indicated by the local minimum in ground range at elevations of 22° (5MHz) or 26° (14MHz)) and/or those rays propagating via the F region to the longest range.

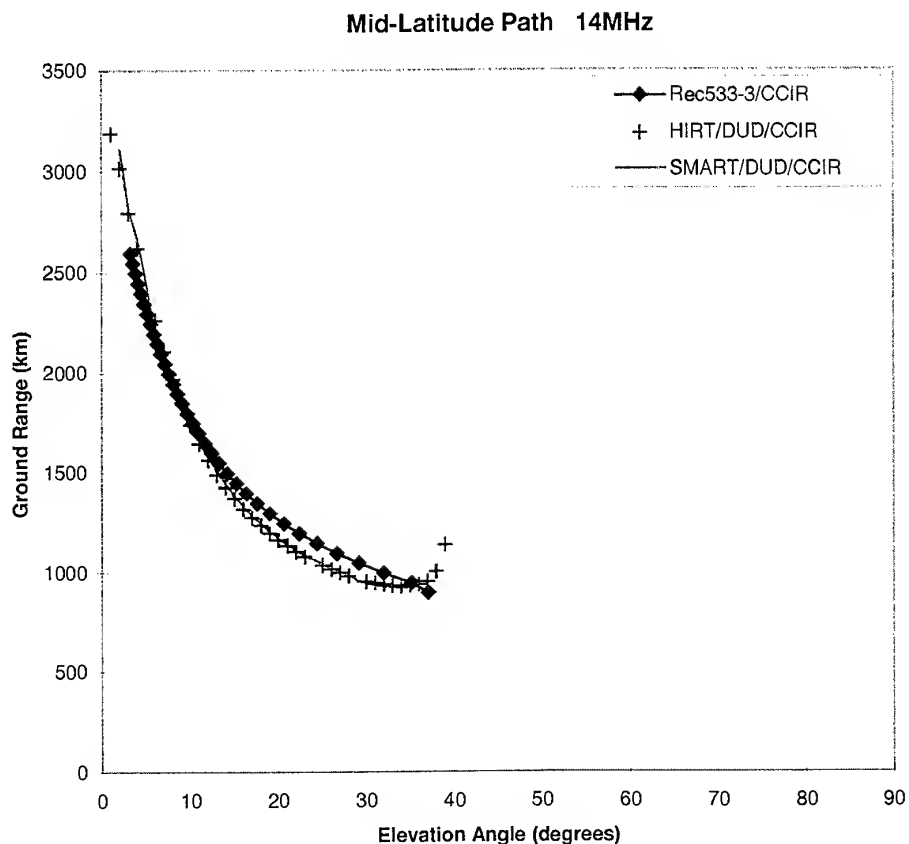


Figure 3-1: Ground range vs. elevation for single-hop, mid-latitude paths launched due south of a transmitter at (55°N, 15°E) at 14 MHz. Results are presented for the ITU Rec533 technique, and analytical (SMART) and numerical (HIRT) ray tracing through a DUD profile fitted to the ionogram-scaled parameters in the ITU database.

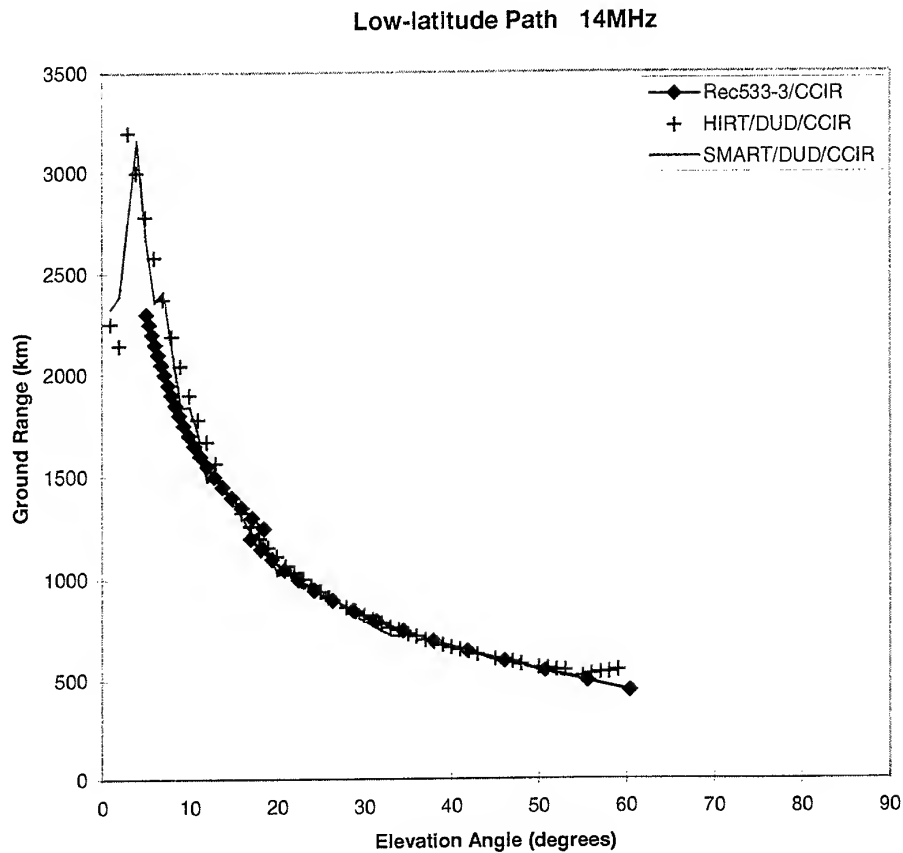


Figure 3-2: Ground range vs. elevation for single-hop, low-latitude paths launched due south of a transmitter at (32°N, 15°E) at 14 MHz. Results are presented for the ITU Rec533 technique, and analytical (SMART) and numerical (HIRT) ray tracing through a DUD profile fitted to the ionogram-scaled parameters in the ITU database.

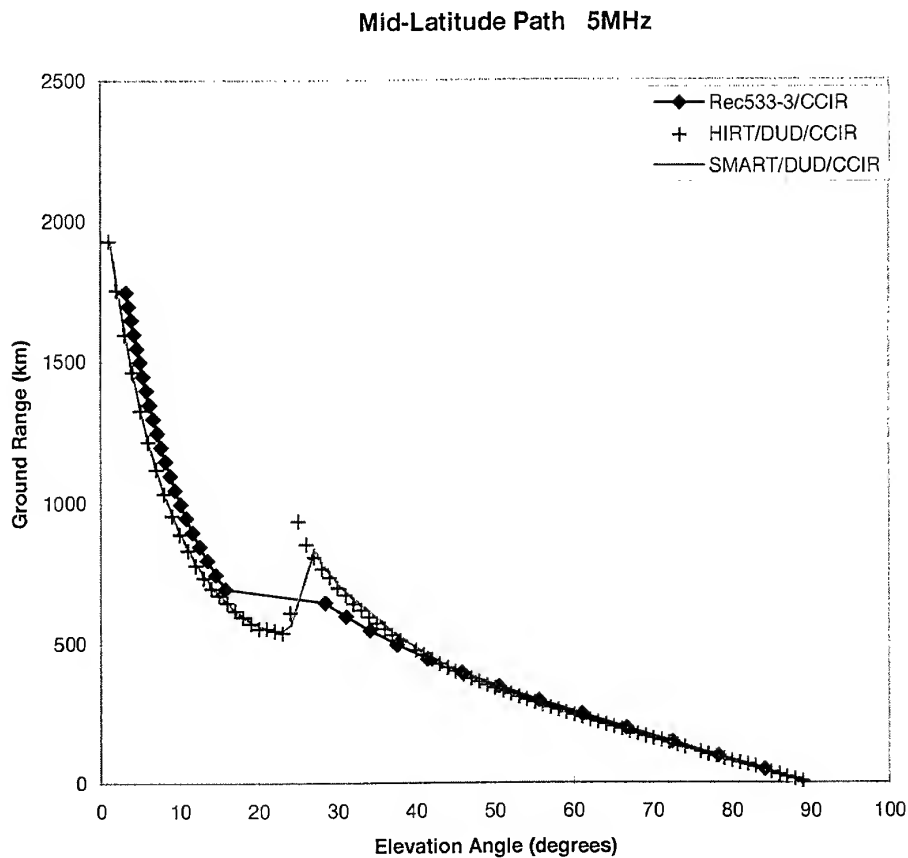


Figure 3-3: Ground range vs. elevation for single-hop, mid-latitude paths launched due south of a transmitter at (55°N, 15°E) at 5 MHz. Results are presented for the ITU Rec533 technique, and analytical (SMART) and numerical (HIRT) ray tracing through a DUD profile fitted to the ionogram-scaled parameters in the ITU database.

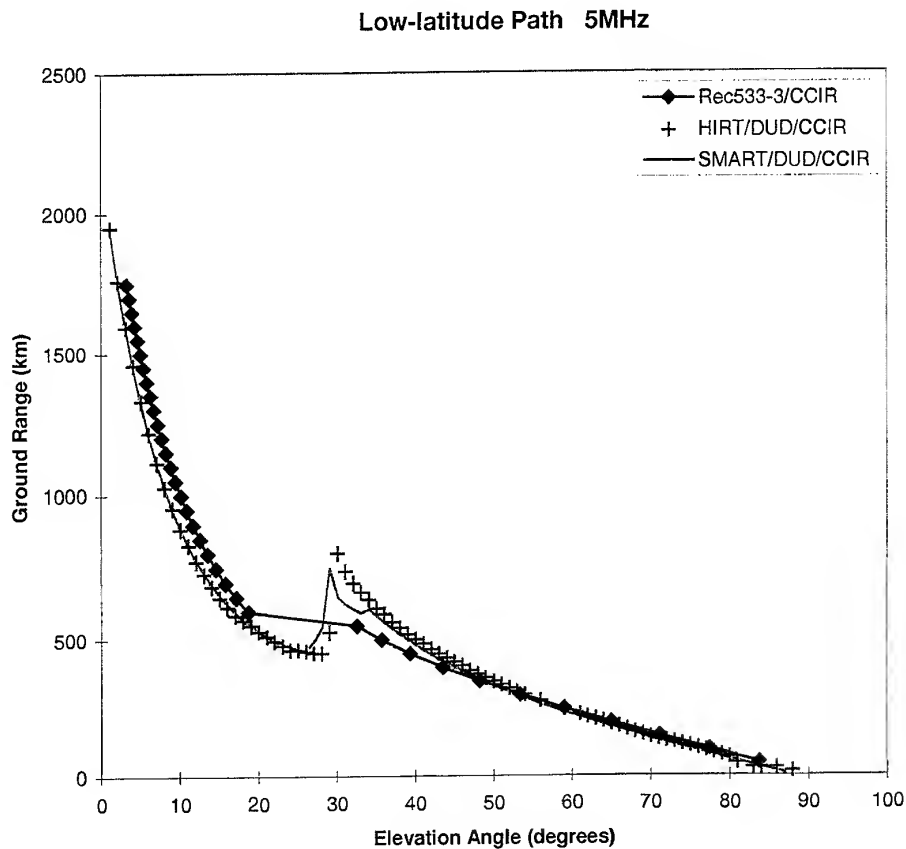


Figure 3-4: Ground range vs. elevation for single-hop, low-latitude paths launched due south of a transmitter at (32°N, 15°E) at 5 MHz. Results are presented for the ITU Rec533 technique, and analytical (SMART) and numerical (HIRT) ray tracing through a DUD profile fitted to the ionogram-scaled parameters in the ITU database.

3.2.2 Table 5 presents a summary of the difference in the ground range between four sample ray traces using SMART and HIRT. Ray tracing was performed at 1° intervals between 1° and 89° elevation through a FAIM model ionosphere at 5MHz and 14MHz at low latitudes (south of (32°N, 15°E)) and mid-latitudes (south of 55°N, 15°E) at 1600UT, in March, with a sunspot number of 122. The mean execution time (per ray) for SMART execution is also presented.

<i>Path</i>	<i>Mid-latitude (south of 55°N, 15°E)</i>		<i>Low-latitude (south of 32°N, 15°E)</i>	
Frequency	5 MHz	14 MHz	5 MHz	14 MHz
Mean difference (%)	4.85	1.85	5.95	2.78
Std. Dev. difference (%)	10.41	1.25	7.82	2.21
Mean absolute difference (km)	44.97	37.15	26.04	31.75
Std. Dev. difference (km)	127.7	34.27	51.50	35.93
Mean SMART execution time per ray (ms)	49.4	96.9	49.4	86.4

Table 5: Mean and standard deviation from mean of differences in the ground range calculations of SMART (analytical ray trace) and HIRT (numerical ray trace). Calculations are based on ray tracing at 1° intervals between 1° and 89° elevation, at 5MHz and 14MHz due south of (32°N, 15°E) (low latitude) and (55°N, 15°E) (mid-latitude) through a FAIM model ionosphere at 1600UT, in March (SSN=122). The mean execution time is also shown.

- 3.2.3 The field strength calculations in Rec533 are semi-empirical in nature and include absorption loss and 'above the MUF' correction terms. However, the other ray-tracing methods in this study predict only the divergent power loss due to radial divergence (free space loss) and any focusing and defocusing of the rays by the ionosphere. In addition, absorption loss is largely dependent on the density of the D region, which is not specified by the physical ionospheric models FAIM or PIM. No direct comparison can therefore be made between the field strength calculations of the Rec.533 method and the other raytracing methods in this study.

4 Integration of PIM/PRISM with SMART

4.1 Implementation

- 4.1.1 In order to maintain the flexibility and portability of the software, it was decided that the ionospheric model and ray tracing algorithms should form two independent modules, with a separate interfacing module used to combine the two. The interface reformats the output from the ionospheric model to produce a three-dimensional electron density grid file in a format accessible to the ray-tracing algorithm. This allows for independent development of the ionospheric model(s). A block diagram of the ionospheric electron density models and ray tracing modules are presented in Figure 4-1.
- 4.1.2 Integration of the PIM model with SMART has been implemented in Version 2.0 of the frequency planning and decision-aid, HF-EEMS (High Frequency Electromagnetic Environment Management System [Shukla *et al.*, 1997]. An example of the SNR maps produced using the ITU Recommendation 533 and the URSI database of ionogram scaled parameters is presented in Figure 4-2 for an transmitter south-west of Greenland, broadcasting at 8 MHz. The corresponding SNR map produced using SMART ray tracing through a PIM ionosphere is presented in Figure 4-3.
- 4.1.3 The absolute level of the signal strength is in error for the SMART/PIM coverage plots and this error is to be rectified in version 2.1 of the software. However, relative differences in the signal strength should not be in error.
- 4.1.4 The SMART/PIM technique clearly displays regions of ray convergence (focussing) near the skip zone (both for single and double hops). This important physical feature is not reproduced by the ITU Rec. 533 technique.
- 4.1.5 Outside the skip zone, the small 'holes' in the coverage of the PIM/SMART SNR maps are due to the finite intervals of elevation angle and azimuth used in the ray trace. The holes are regions where no ray landed in the 2D grid of latitude and longitude on the ground.

4.2 Suggestions for Future Research

- 4.2.1 Holes in the coverage area could be avoided by increasing the size of the cells on the map, (resulting in lower resolution), or by reducing the launch elevation and azimuth angle increments of the rays (resulting in longer computation time).
- 4.2.2 Isolated holes could be filled by interpolation with surrounding grid elements. Another approach might involve tagging each cell with the launch azimuth and elevation of the ray that landed in it and interpolation to find the most probable launch azimuth and elevation of the rays that might land in the holes.
- 4.2.3 Alternatively, the homing procedure described in Section 5 might be applied to search for solutions to those empty cells lying beyond the inner skip zone. If homing were used for all cells in the map, it could provide maps of predicted multipath delay spread for a given maximum range of signal strengths (or *vice versa*). This could be used to select an appropriate modem on an HF communications link. However, the homing procedure is a time consuming and inefficient process for coverage maps since most of the results are discarded.

- 4.2.4 One last consideration is the design of the coverage map. Currently this is divided into cells bounded by lines of geographic latitude and longitude. There is no inherent reason for this and it limits the azimuthal resolution of the signal coverage map at close range whilst producing holes at long range. If a two dimensional ray trace such as SMART is used then the map should be divided into cells bounded by lines of range and azimuth from the transmitter. The azimuth intervals would be set identical to those of the ray trace.

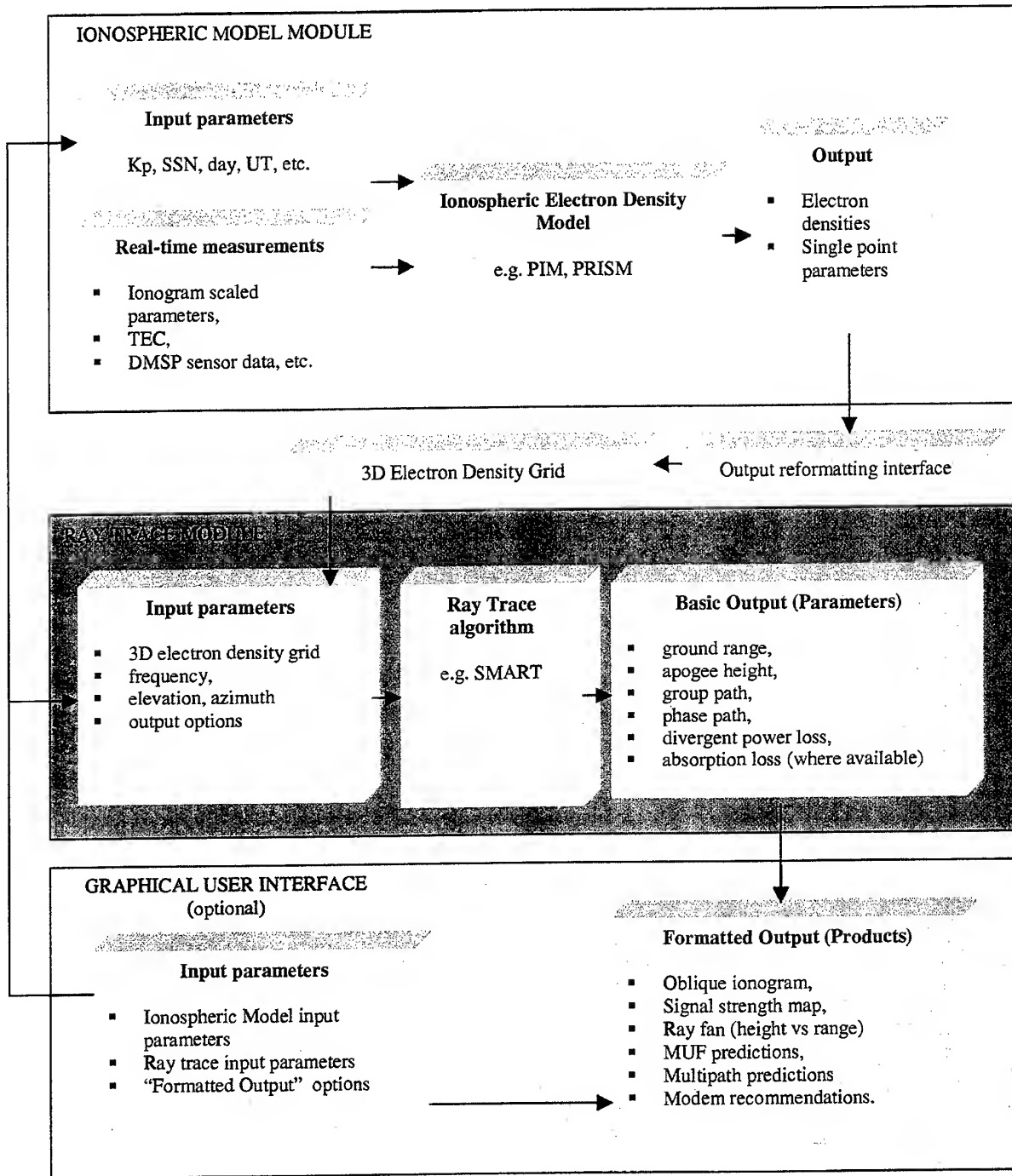


Figure 4-1: Block diagram to illustrate the integration of ray tracing and ionospheric models.

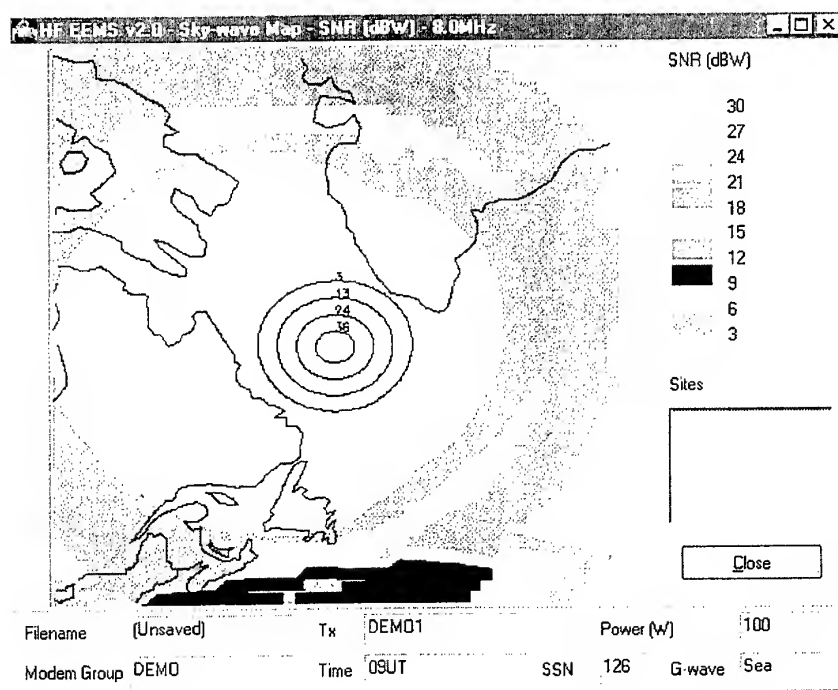


Figure 4-2: Sample SNR coverage map from HF-EEMS, created using the ITU Recommendation 533 and the URSI database of ionogram scaled parameters. Ground-wave SNR contours are also shown (as rings).

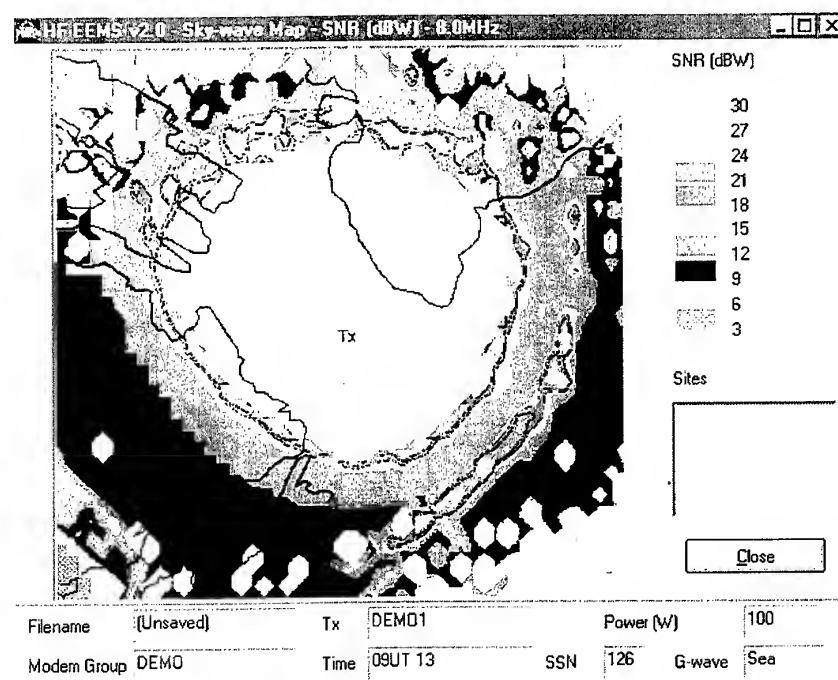


Figure 4-3: Sample SNR coverage map from HF-EEMS, created using the SMART ray tracing algorithm and the PIM ionospheric model. Driving parameters are identical to those of Figure 4-2. Note: the ground wave SNR contours are not shown.

5 Synthesis of Oblique Ionograms by Ray Tracing

5.1 Introduction

5.1.1 To validate the ionospheric electron density model, a direct comparison was required between the results of ray traces through the model with simultaneously recorded IRIS oblique ionograms. For this purpose, a homing technique - developed by DERA as part of another programme of research - was used in conjunction with the analytical ray tracing code to generate synthetic oblique ionograms. This technique is described below.

5.1.2 The user of the computer program specifies an azimuth and range, R_h , or a receiver location upon which to home. If the latter is specified, the azimuth and range are determined automatically by spherical trigonometrical calculations. The user must also provide a tolerance on the homing range, dR_h , to enable the program to return values with a finite error. dR_h was set to 2 km in this study.

$\beta_{low}, R_{low}, (dR/d\beta)_{low}$	launch elevation angle, ground range and rate of change of range with launch angle of lower elevation ray
$\beta_{high}, R_{high}, (dR/d\beta)_{high}$	launch elevation angle, ground range and rate of change of range with launch angle of higher elevation ray
$\beta_{mid}, R_{mid}, (dR/d\beta)_{mid}$	launch elevation angle, ground range and rate of change of range with launch angle of ray lying between higher and lower rays
R_h	Homing range
dR_h	+/- tolerance on homing range

Table 6: Definition of symbols used in description of the homing procedure.

5.1.3 A flow diagram for the homing algorithm as implemented in the software is presented in Appendix A and the procedure is explained below. Ray tracing is first performed at two launch elevation angles, $\beta_{high}=90^\circ$, and $\beta_{low}=85^\circ$. If the ground range of either of these rays lies in the interval $R_h \pm dR_h$, then the program writes a record containing fields of frequency, elevation, range, apogee height, group path, phase path, and power loss for that ray. The range R and rate of change of range with launch angle, $dR/d\beta$ (hereinafter referred to as the 'gradient'), are calculated directly from the analytical raytrace equations for each of the two rays. These values are passed to a recursive subroutine called HOME2, which returns with the actions listed in Table 7.

Condition number	Low elevation ray		High elevation ray		Action	Comments
	R	dR/d β	R	dR/d β		
1	penetrate	-	penetrate	-	-	-
2	$> R_h$	> 0	$> R_h$	< 0	-	R high, local max
3	$< R_h$	< 0	$< R_h$	> 0	-	R low, local min
4	$< R(\text{high})$	> 0	$< R_h$	> 0	-	R low, increasing
5	$> R(\text{high})$	< 0	$> R_h$	< 0	-	R high, decreasing
6	$> R_h$	> 0	$> R(\text{low})$	> 0	-	R high, increasing
7	$< R_h$	< 0	$< R(\text{low})$	< 0	-	R low, decreasing
8	$> R_h$	< 0	$< R_h$	< 0	linear interpolation	R decreasing below R_h
9	$< R_h$	> 0	$> R_h$	> 0	linear interpolation	R increasing above R_h
10	NONE OF THE ABOVE				bisection	-

Table 7: Actions performed during the homing technique. The range, R , and rate-of-change of R with launch angle, β , are calculated and compared with the homing range, R_h . No action implies cessation of homing on the interval, otherwise the interval is divided into two parts and homing performed on each sub-interval.

5.1.4 The condition numbers in Table 7 are explained below.

5.1.5 No action is taken and homing is aborted on the elevation angle interval if one of the following conditions occur,

1. Both rays penetrate the ionosphere.
2. Both rays have range greater than the homing range and gradients imply a local range maximum in the interval.
3. Both rays have range less than the homing range, and gradients imply a local range minimum in the interval.
4. Both rays lie below the homing range, the range increases with the increase in elevation and gradients are positive for both rays.
5. Both rays lie above the homing range, the range decreases with the increase in elevation and gradients are negative for both rays.
6. Both rays lie above the homing range, the range increases with the increase in elevation and gradients are positive for both rays.
7. Both rays lie below the homing range, the range decreases with the increase in elevation and gradients are negative for both rays.

5.1.6 If any of the following conditions hold true, the elevation interval is intersected by linear interpolation to R_h .

8. The low elevation ray lands at a range greater than the homing range, the high elevation ray lands at a range less than the homing range, and the gradients are both negative.

9. The low elevation ray lands at a range less than the homing range, the high elevation ray lands at a range greater than the homing range, and the gradients are both positive.

5.1.7 If none of the above conditions are met, the elevation angle interval is bisected and another ray trace performed for the bisecting ray. HOME2 is then recursively called on these two intervals. Examples of this could include the following,

- Either (but not both) rays fail (e.g. one ray penetrates).
- Both rays have range $< R_h + dR_h$ and gradients imply a local range maximum (i.e. $(dR/d\beta)_{low} > 0$ and $(dR/d\beta)_{high} < 0$).
- Both rays have range $> R_h + dR_h$ and gradients imply a local range minimum (i.e. $(dR/d\beta)_{low} < 0$ and $(dR/d\beta)_{high} > 0$).
- Gradients have the same sign but range does not vary in same sense as the gradients (i.e. gradients both have the opposite sign to $R_{high} - R_{low}$). (This implies an N or inverted-N discontinuity in the range vs. elevation plane.)

5.1.8 If at any time, a ray is calculated to have a range within the required homing range ($R_h \pm dR_h$) a record is written containing fields of frequency, elevation, range, apogee height, group path, phase path, and power loss.

5.1.9 The recursive routine HOME2 is subsequently repeated for all 5° intervals down from 85° to 0° elevation.

5.1.10 An example of a typical homing procedure is presented in Figure 5-1. At low elevations, propagation is supported from E-layer reflections, whereas at higher elevations the E region is penetrated and signals are reflected from the F region. At the highest elevations the ray penetrates the ionosphere completely.

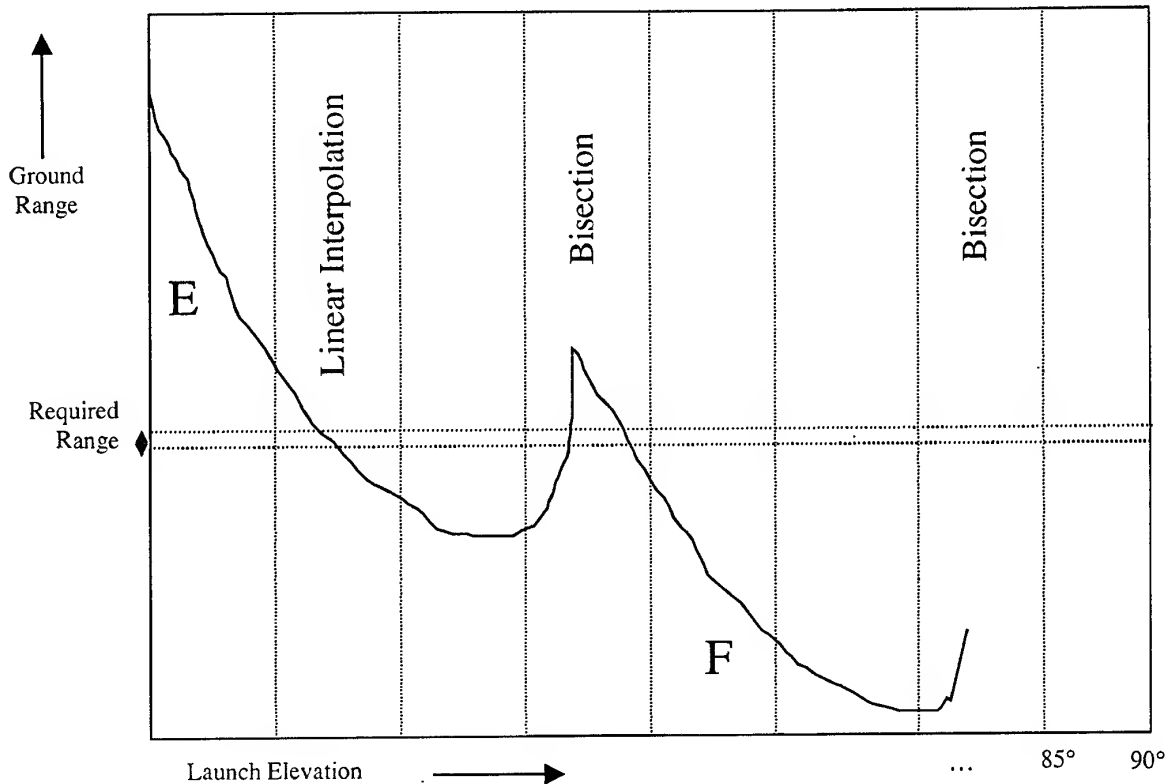


Figure 5-1 Diagram to illustrate the design of the homing procedure. Homing is performed on 5° intervals of the launch elevation angle. In this example, homing is performed in only three intervals of elevation angle.

- 5.1.11 The main disadvantage of this homing algorithm is the fact that the bisection homing routine is applied where one ray of a pair either has no analytical solution or penetrates the ionosphere. The program will continuously bisect the interval until it comes within 0.01° of the penetration angle. Though robust, this method often consumes the majority of the computer processing time.
- 5.1.12 When used to synthesise oblique incidence ionograms the homing procedure is performed at 0.1MHz intervals upwards of 2MHz. To save computer processing time, the program is aborted at a frequency greater than 2MHz above the frequency of the last successfully homed ray.
- 5.1.13 Several tests were performed to verify the operation of the homing procedure. A synthesised oblique ionogram was generated for a particular transmitter-receiver path and the results were compared with those obtained using a 'full ray fan' method. In the latter, ray tracing was performed at 0.05° intervals over all elevation angles and the ray parameters written to a file, a process requiring about 2 hours of computer processing on a PC with a Pentium 90MHz CPU processor (This compared to approximately 1 minute for the homing method). The output file was then filtered for rays of the correct range and the corresponding group delays ($= [\text{group path}] / [\text{speed of light in free space}]$) plotted against frequency to form the ionogram. The two methods produced virtually indistinguishable results.

6 Validation of ionospheric models using IRIS Ionograms

6.1 Introduction

6.1.1 The use of the UK IRIS oblique sounder network has been used extensively to validate and develop the accuracy of tomographic images in another programme of research at DERA. The main findings of this research were presented by *Rogers et al.* [1999]. This section describes some of the methods and results of the ionospheric tomography project and extends these to include assessments of ITU Recommendation 533 and the PRISM model.

6.2 Methodology

6.2.1 The ionospheric electron density models to be validated using oblique ionogram data were as follows:

- Tomographic image produced from UK chain of receivers.
- Tomographic image with electron density profile from Chilton ionosonde incorporated in the reconstruction.
- Tomographic image utilising both Chilton and Lerwick ionosonde information
- Parameterised Ionospheric Model (PIM) [*Daniell et al.*, 1995]
- Fully Analytical Ionospheric Model, FAIM [*Anderson et al.*, 1989]
- International Reference Ionosphere model (IRI-95) [*Bilitza*, 1990; *Rawer et al.*, 1995, 1996]
- Parameterised Real-time Ionospheric Specification Model (PRISM) [*Daniell*, 1991], with additional real-time parameters derived from the Chilton and Lerwick ionograms

6.2.2 Each model generated electron densities at 5km height intervals and 0.25° latitude and longitude intervals.

6.2.3 Synthesised ionograms were produced by ray tracing at the nine times listed in Table 8 and compared with IRIS oblique sounder ionograms on all six paths of the UK IRIS network.

Date	Day	UT	SSN (27-day average)	kp	By
28/03/98	87	07:42	65.96	1.7	
02/04/98	92	07:04	68.26	0.3	+
02/04/98	92	07:29	68.26	0.3	+
06/04/98	96	15:13	64.67	0.3	+
12/04/98	102	06:40	58.04	1.3	
17/04/98	107	06:28	52.93	2.7	+
20/04/98	110	06:00	54.07	2.3	-
23/04/98	113	02:09	50.63	1.7	
23/04/98	113	17:41	50.63	0.7	
23/04/98	113	17:59	50.63	0.7	
25/04/98	115	05:48	48.04	4.0	
28/04/98	118	17:46	45.85	1.7	-
30/04/98	120	05:36	46.85	0.7	+
01/05/98	121	17:00	48.19	1.3	+

Table 8: Times of tomographic images and ionospheric electron density models used in the oblique ionogram comparisons. Values of the sunspot number (SSN) (27-day running mean), kp index and the sign of the dawn-dusk component of the interplanetary magnetic field (B_y) used in the comparative ionospheric models are also presented. Where IMF measurements were unavailable B_y was set negative by default. B_z values were set negative throughout since in PIM the kp value defaults to 1.0 where positive values of B_z are used.

6.2.4 In order to quantify the level of agreement between the synthesised and measured traces, six parameters were scaled from the single-hop traces on each ionogram (see Figure 6-1). These were $f_{min}(F)$, the minimum observed frequency of the F trace, MUF(E) and MUF(F2), the maximum frequencies of the E and F2 traces, respectively, and m'd(E), m'd(F1) and m'd(F2), the minimum absolute time delay of the E, F1 and F2 traces respectively. Where there was no clear division of the F region, the minimum delay of the F trace was recorded as m'd(F1) and m'd(F2) was not scaled.

6.2.5 In Figure 6-1 two ionogram traces are observed separated by about 0.7MHz. This is due to magneto-ionic splitting of the ray as it passes through the magnetised plasma of the ionosphere. The lower frequency trace is called the o-ray and is unaffected by the magnetic field. The ray trace equations of SMART assume a zero magnetic field, so only the o-ray traces are scaled from the ionograms.

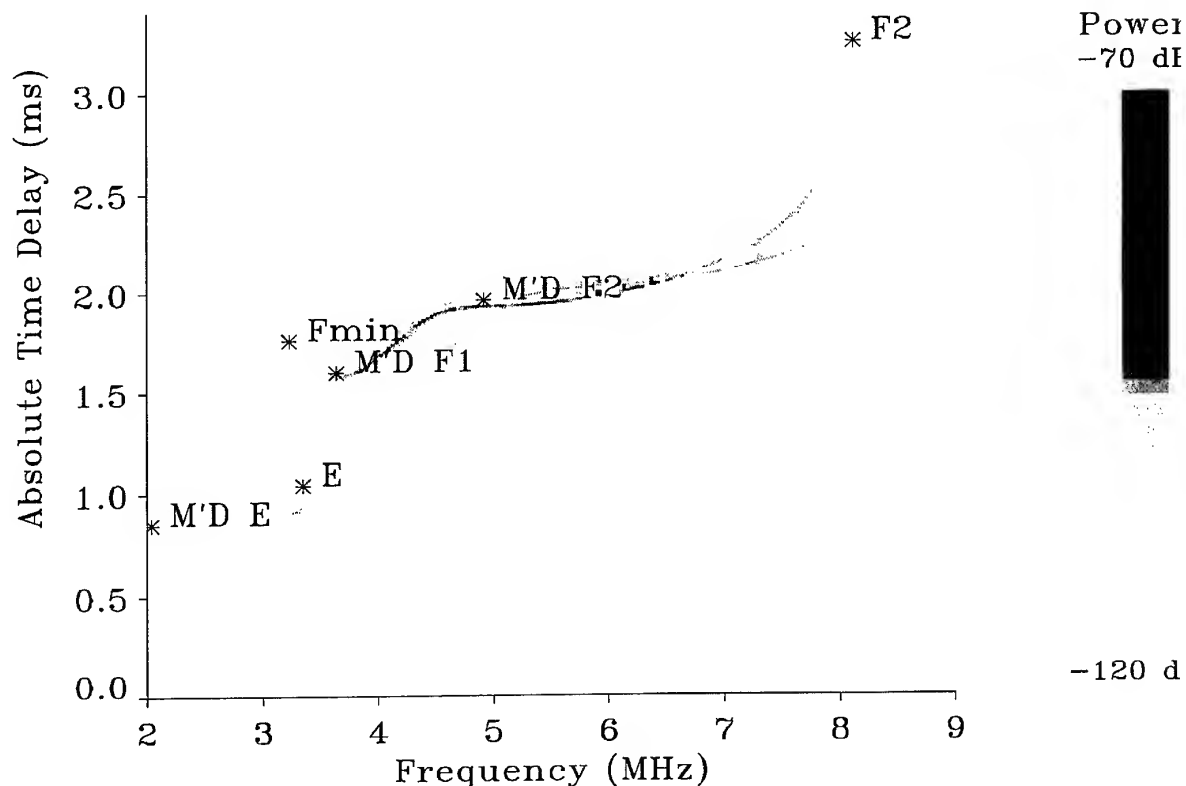


Figure 6-1: IRIS oblique ionogram for the Cove-Malvern path on 6/4/98 at 1516UT. The six scaled parameters ($f_{min}(F)$, $MUF(E)$, $MUF(F2)$, $m'd(E)$, $m'd(F1)$ and $m'd(F2)$) are indicated by the asterisks labelled F_{min} , E , $F2$, $M'D E$, $M'D F1$ and $M'D F2$ respectively.

6.3 Results

- 6.3.1 The mean percentage overestimates of the ionogram scaled parameters comparisons (synthetic ray traced parameters relative to measured IRIS parameters) are presented in Figure 6-2 and Figure 6-4. The root-mean-square errors for each parameter are presented in Figure 6-3 and Figure 6-5. These charts also include parameters obtained from the ITU Rec. 533 ('virtual mirror') technique.

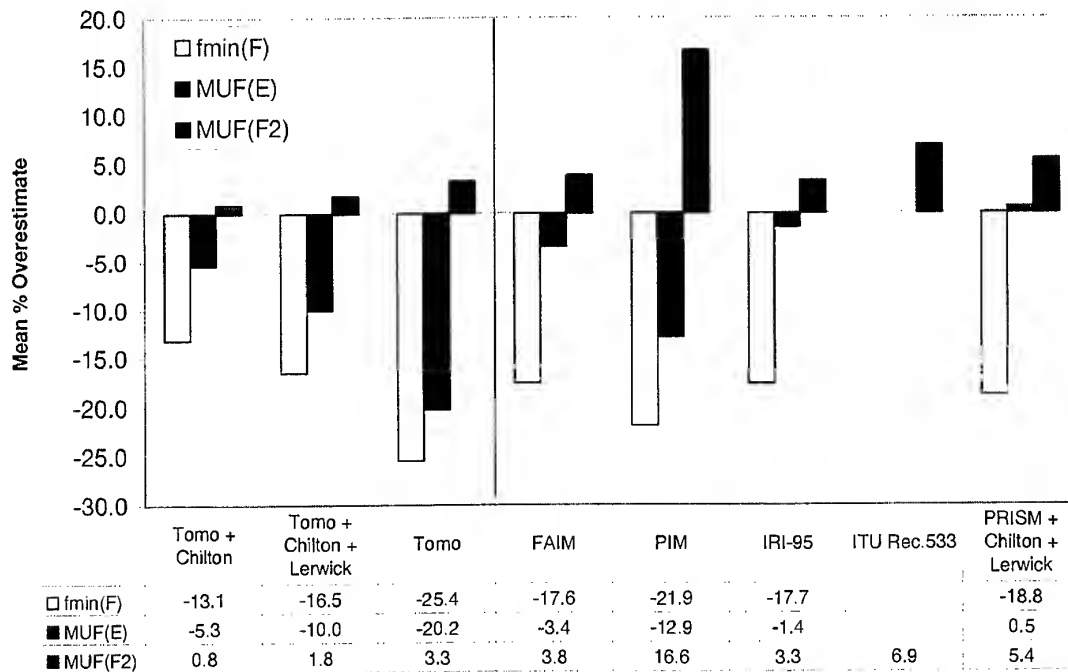


Figure 6-2: Mean percentage overestimates of synthetic oblique ionogram scaled frequency parameters (with respect to IRIS measured values) by ray tracing through three ionospheric models. Results are based on times of propagation listed in Table 8.

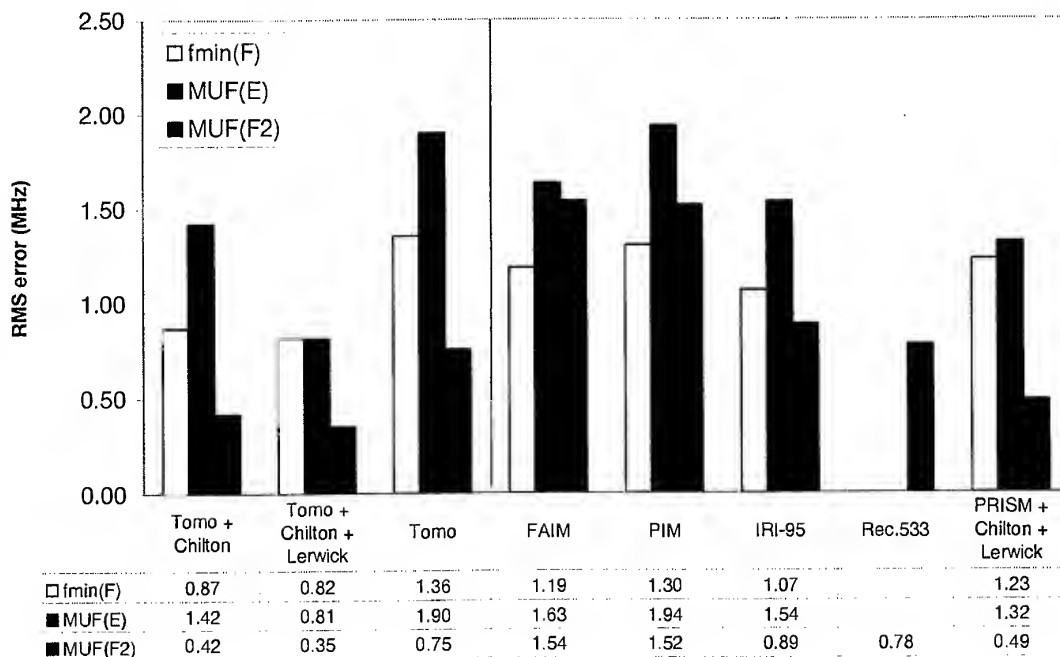


Figure 6-3: Root-mean-square errors of synthetic oblique ionogram scaled frequency parameters (with respect to IRIS measured values) by ray tracing through three ionospheric models. Results are based on times of propagation listed in Table 8.

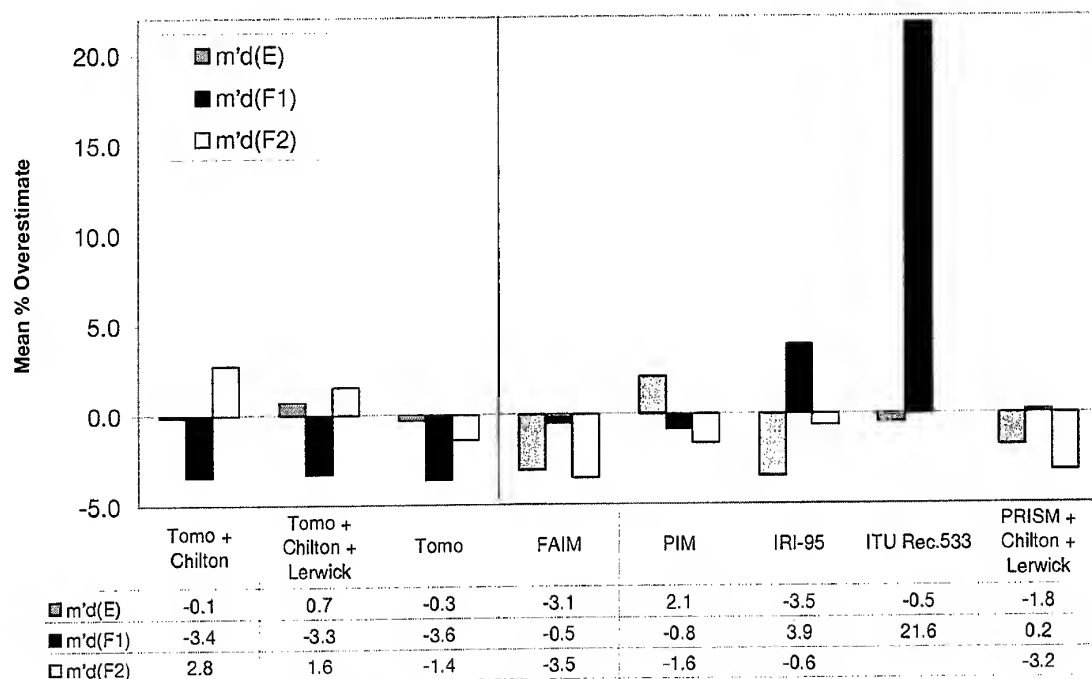


Figure 6-4: Mean percentage overestimates of synthetic oblique ionogram scaled delay parameters (with respect to IRIS measured values) by ray tracing through three ionospheric models. Results are based on times of propagation listed in Table 8.

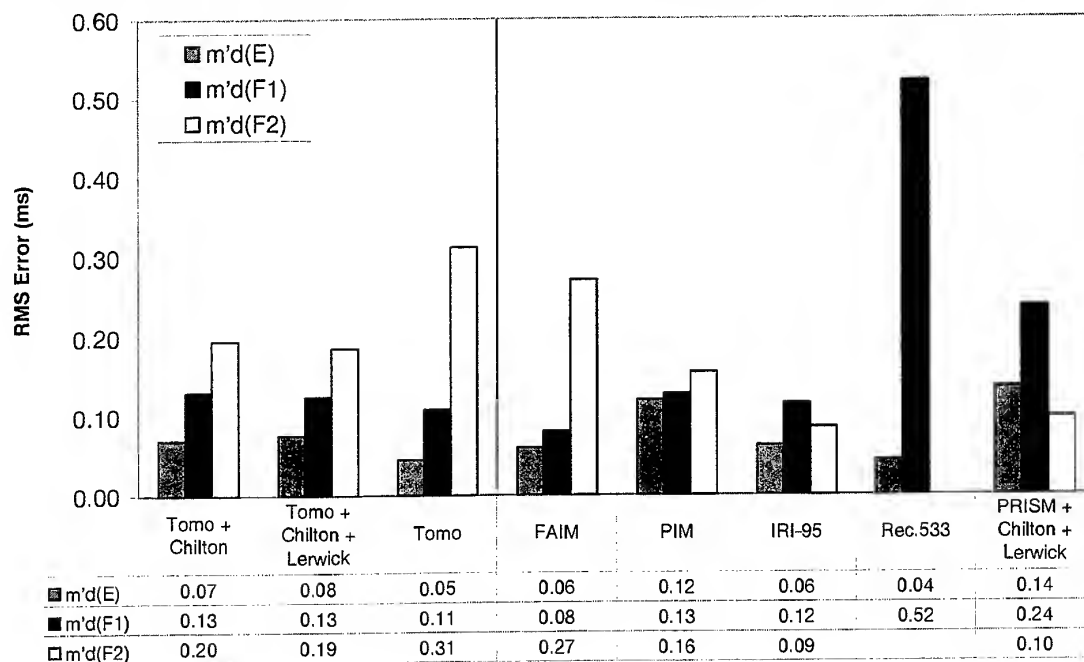


Figure 6-5: Root-mean-square errors of synthetic oblique ionogram scaled delay parameters (with respect to IRIS measured values) by ray tracing through three ionospheric models. Results are based on times of propagation listed in Table 8.

6.3.2 MUF comparisons

- 6.3.2.1 The mean percentage overestimates of each of the three frequency scaled ionogram parameters are presented in Figure 6-2 with root mean square errors presented in Figure 6-3. With the exception of PRISM the E region MUF is underestimated, and F-region MUFs are overestimated in every case.
- 6.3.2.2 Three methods of tomographic reconstructions are presented, the first incorporates electron density profiles deduced from the Chilton ionograms using the POLAN inversion procedure. The second also includes the electron density profile at Lerwick and the third is the tomographic reconstruction from TEC measurements alone (*i.e.* with no ionosonde input). With no sounder measurements the MUF(E) is, on average, underestimated by 20%, and the RMS error is 1.9MHz. Inclusion of the Chilton ionosonde reduces the average error to 5% and lowers the RMS error. Inclusion of a second ionosonde at Lerwick leads to deterioration of the mean MUF(E) errors, but an improvement on the RMS error.
- 6.3.2.3 In tomography an underestimated E-region peak density would result in a redistribution of plasma to higher altitudes to compensate for the TEC. Thus a low estimate of MUF(E) would increase the estimated MUF(F2), and this is observed as an anti-correlation between E and F-region MUF errors for the three tomographic methods presented. It is uncertain how much this effect would be offset by reduced E-region refraction and hence lower angles of incidence, i , on the F region which would tend to reduce the MUF(F2) (since MUF is roughly proportional to $\sec(i)$).
- 6.3.2.4 The FAIM, IRI-95 and PRISM models all reduce the mean error of MUF(E) compared with Tomography. However, the PIM model exhibited a relatively large mean underestimate of 12.9%. Whilst these experiments cannot be considered a comprehensive assessment of the climatological models, it has been suggested by the authors of PIM, [*R. Daniell and D. Decker, private communication, 1999*] that better results might be achieved by normalising the foF2 values to the URSI-88 global database of ionogram scaled parameters. (The contrary option, recommended in the PIM 1.6 user guide, was used in this study).
- 6.3.2.5 The MUF(F2) estimates based on the tomographic reconstructions are superior to those resulting from the climatological model predictions, both in the average and RMS sense. Of the models, IRI-95 produced the least error in MUF(F2) (3.3% overestimate) whilst PIM produced the worst estimate of this parameter (16.6% overestimate),
- 6.3.2.6 The RMS error in both the MUF(E) and MUF(F2) measurements is generally higher for the climatological models than for those incorporating real-time ionosonde measurements (Tomography and PRISM). This emphasises the fact that real-time measurements are necessary to reproduce the inherent variability of the ionosphere.

6.3.3 Fmin(F) comparisons

- 6.3.4 The mean overestimate and RMS error of parameter fmin(F), the minimum observable frequency of the F-trace, are represented by the light yellow bars of Figure 6-2 and Figure 6-3 respectively. The parameter fmin(F) is effectively a measure of the foE at the path midpoint and was only scaled when a clear frequency cut-off was observed (*i.e.* at the point of asymptotic group retardation). Fmin(F) was more difficult to scale on the longer paths. Fmin(F) was underestimated in all cases. Comparing results from the tomographically imaged ionospheres, the errors diminish slightly when ionosonde

electron density profiles are included in the reconstruction though the improvement over climatological models is still only marginal.

6.3.5 Minimum trace delay comparisons

6.3.6 Statistical comparisons of the minimum delay ($m'd$) of E, F1 and F2 traces are presented in Figure 6-4 (mean percentage errors) and Figure 6-5 (RMS errors). On average, the errors in $m'd(E)$ are smaller for tomographic techniques (up to 0.7% error) than for climatological models (up to 3.5% error). ITU Rec.533 predicts the minimum delay of the E trace better than any model, with a mean error of just -0.5%. This model simply sets the 'virtual' reflection point of the E layer to 110km altitude.

6.3.7 Values of $m'd(F1)$ are persistently underestimated by tomographic techniques (by 3.3 to 3.6%), whereas the climatological models FAIM, PIM and PRISM produced average errors of less than 0.8%. This suggests that the tomographic reconstructions are underdense in the E and/or E-F valley regions of the ionosphere (since higher densities lead to greater group retardation). ITU Rec. 533 grossly overestimates $m'd(F1)$ (by 21.6%).

6.4 Case Study: Synthetic and measured ionograms on the Cove Malvern path – 6th April 1998, 1516UT.

6.4.1 The scaled parameters of a synthetic ionogram provide only a crude indication of the accuracy of the ionogram as a whole.

6.4.2 In Figure 6-6 to Figure 6-9, synthesised ionograms (green triangles) are presented for the Cove-Malvern path at 15:16UT on the 6th April 1998. These are produced by ray tracing through models FAIM and PIM and tomographic images obtained first without and then with the inclusion of an electron density profile from the Chilton ionosonde in the reconstruction. These are all superimposed on the ionogram from the IRIS receiver.

6.4.3 In this example, the two climatological models reproduce the E and lower F1 mode ionogram traces with great accuracy. The upper F1 and F2 traces, however, are poorly reproduced and there is no clear division between F1 and F2 traces. The mid-point electron density profiles are presented in Figure 6-10. Neither model exhibits a clear F1 ledge.

6.4.4 The tomographic reconstructions both correctly place the minimum delay of the E trace, but the delay is overestimated at higher frequencies on the E trace. The associated mid-point electron density profiles in Figure 6-11 show that the peak of the E layer lies at 125km altitude, which is 10-15km higher than in the climatological models. The F1 ledge in the electron density profile and the corresponding 'step' between the F1 and F2 traces in the ionogram is only reproduced when the electron density profile from Chilton is included in the tomographic reconstruction.

6.4.5 Figure 6-12 presents the predictions of the ITU Rec. 533 as green triangles, superimposed on the IRIS ionogram for the Cove-Malvern path. The accuracy of the MUFs of the E and F2 modes are comparable with other models (see Figure 6-2 and Figure 6-3) and the E mode delay (corresponding to a fixed virtual height of 110km) is very close to that observed. However, the group delay of the F region is not accurately predicted since Rec.533 does not incorporate parameters of the F1 region and relies on an empirical method of calculating the virtual height of reflection. Other tests have shown the virtual height of the F2 region to vary with frequency, but the resulting 'ionograms' do not appear realistic or accurate when compared with IRIS ionograms.

- 6.4.6 Errors in the virtual reflection height of the F region translate directly into ground range errors and inaccuracies in the predictions of broadcast HF signal coverage.
- 6.4.7 The ITU Rec.533 predictions for the longer (763km) Lancaster – Saxa Vord path are compared with IRIS measurements in Figure 6-13. The E trace delay is again well represented by the simple 110km virtual mirror height of Rec533, but the F-region delays are greatly overestimated. The Rec.533 method always selects the F2 mode when the frequency exceeds the E layer screening frequency. This inevitably leads to errors in the geographical pattern of HF signal coverage.

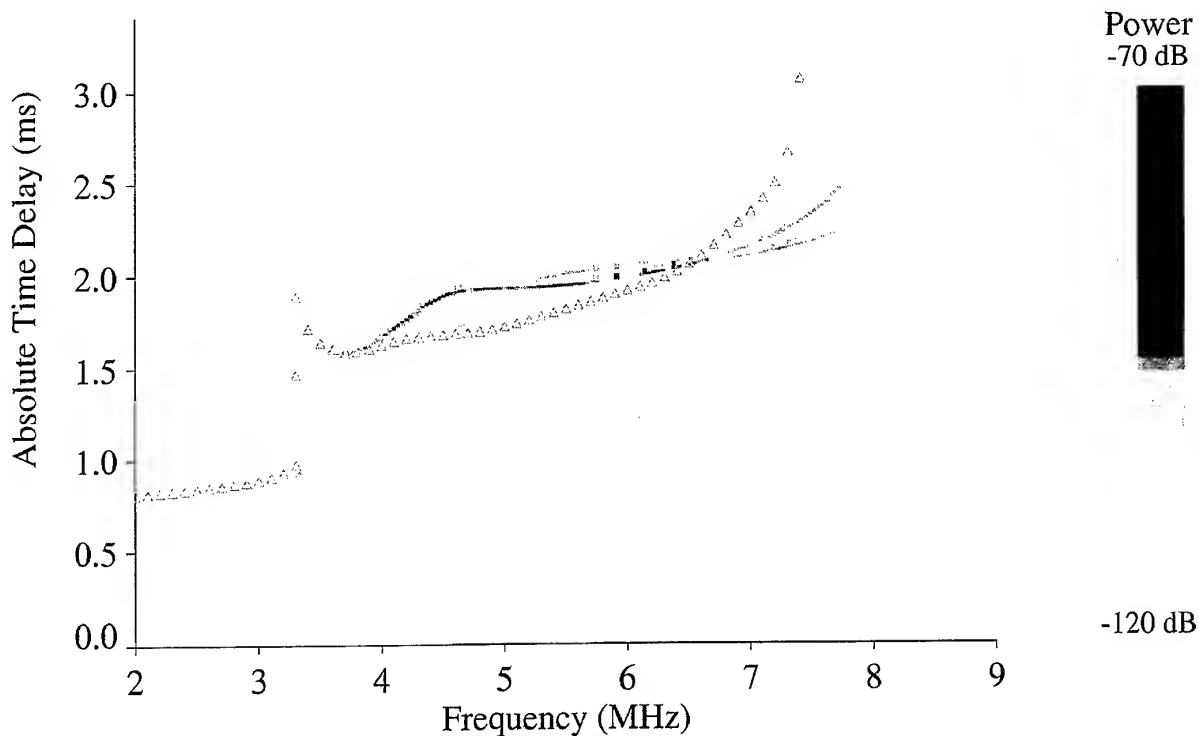


Figure 6-6: IRIS ionogram recorded on the Cove-Malvern path at 15:16UT on 6th April 1994. Green triangles represent synthetic ionogram produced by ray tracing through the FAIM model.

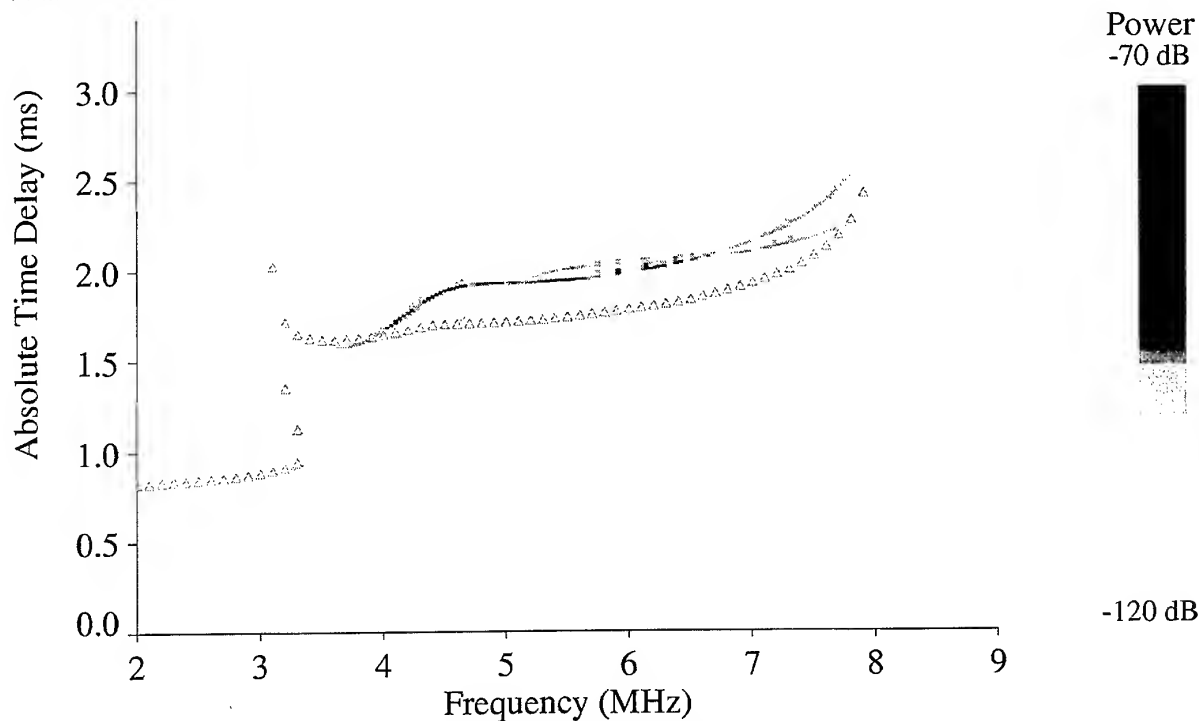


Figure 6-7: IRIS ionogram recorded on the Cove-Malvern path at 15:16UT on 6th April 1994. Green triangles represent synthetic ionogram produced by ray tracing through the PIM model.

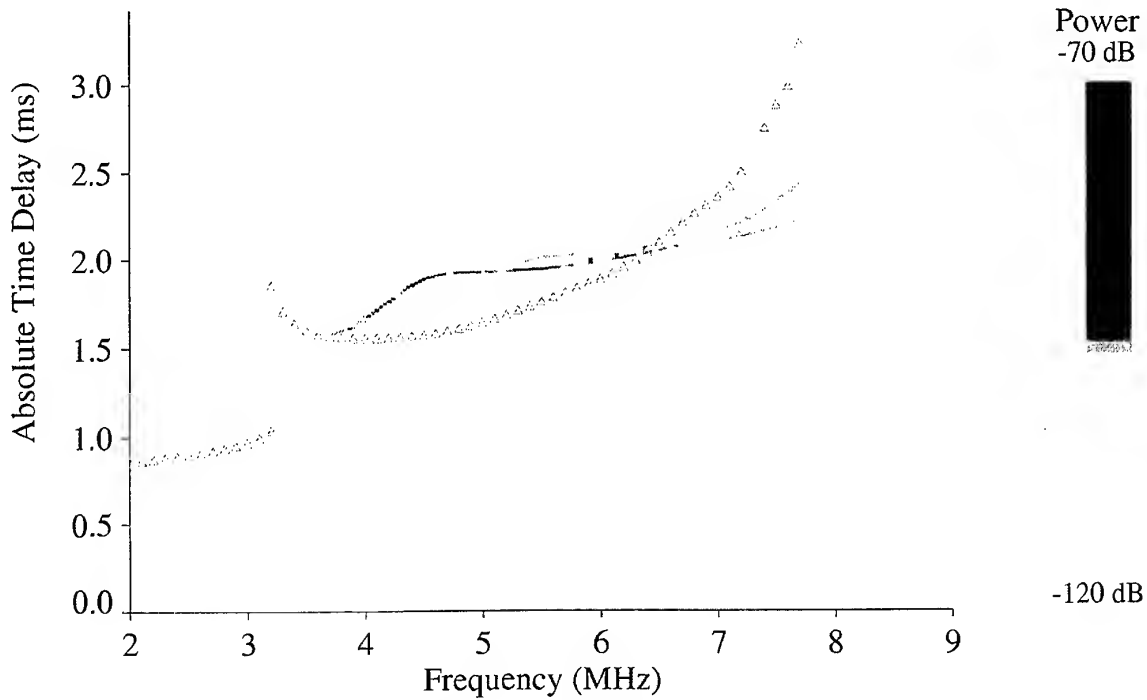


Figure 6-8: IRIS ionogram recorded on the Cove-Malvern path at 15:16UT on 6th April 1994. Green triangles represent synthetic ionogram produced by ray tracing through a tomographic image produced with no additional measurements from vertical ionosondes.

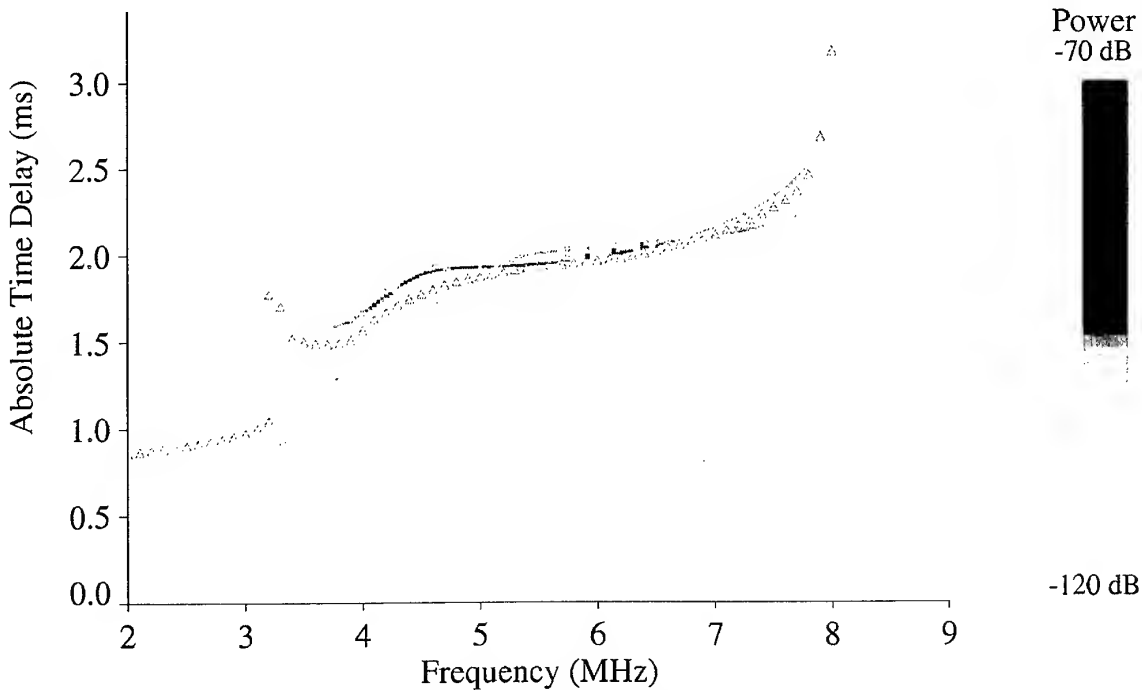


Figure 6-9: IRIS ionogram recorded on the Cove-Malvern path at 15:16UT on 6th April 1994. Green triangles represent synthetic ionogram produced by ray tracing through a tomographic image produced using measurements from the Chilton vertical ionosonde.

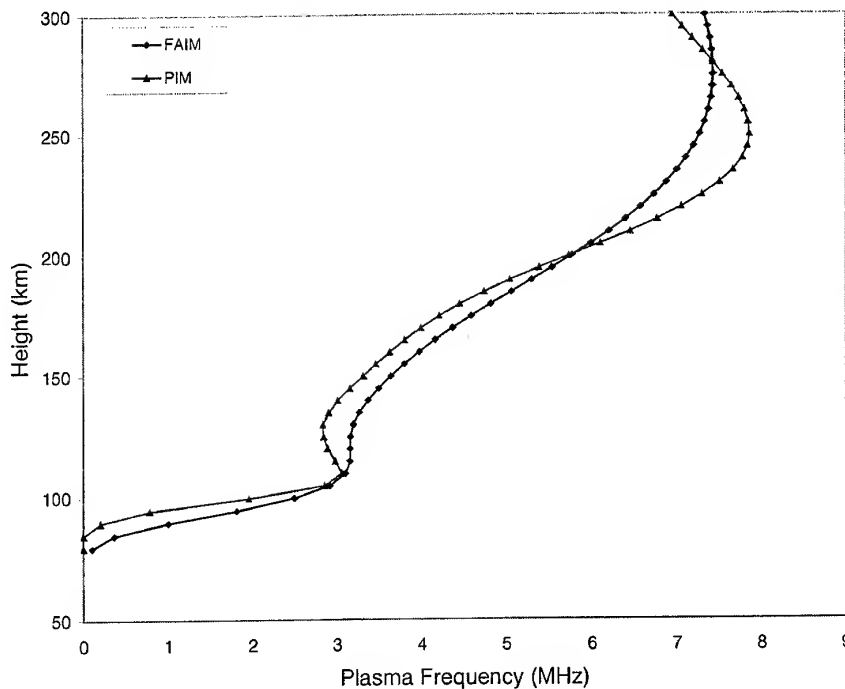


Figure 6-10: FAIM and PIM model plasma frequency profiles at the mid-point of Cove-Malvern path at 15:16UT on 6th April 1998.

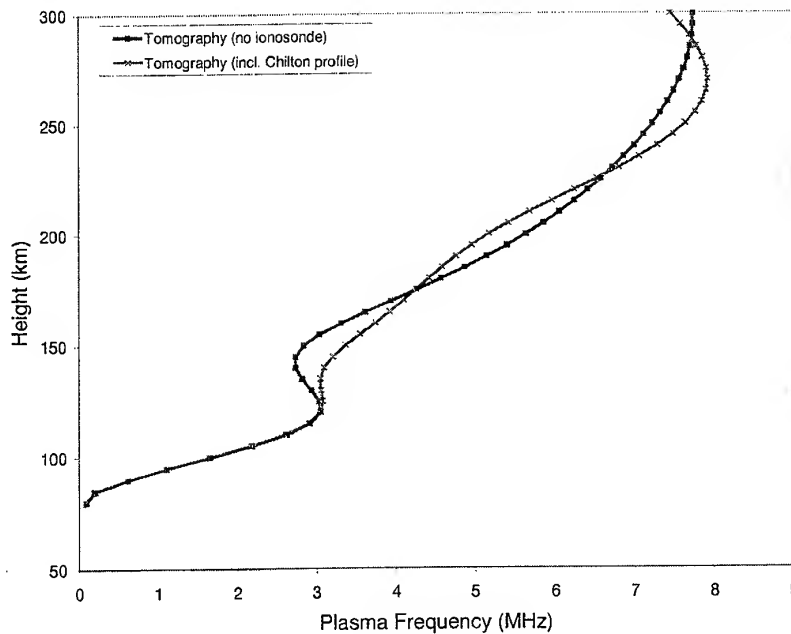


Figure 6-11: Plasma frequency profiles from tomographic images at the mid-point of the Cove-Malvern path at 15:16UT on 6th April 1998. The two lines represent profiles from the tomographic images reconstructed with and without the incorporation of POLAN electron density profiles from Chilton sounder.

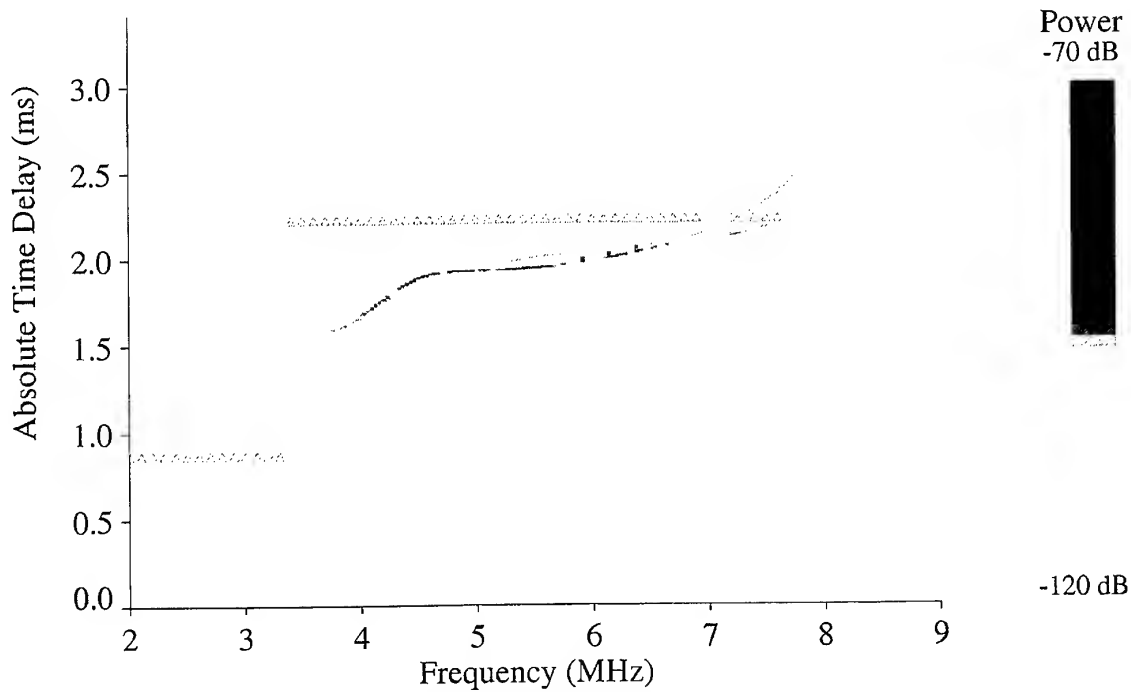


Figure 6-12: IRIS ionogram recorded on the Cove-Malvern path at 15:16UT on 6th April 1994. Green triangles represent predictions of the ITU Rec. 533 model.

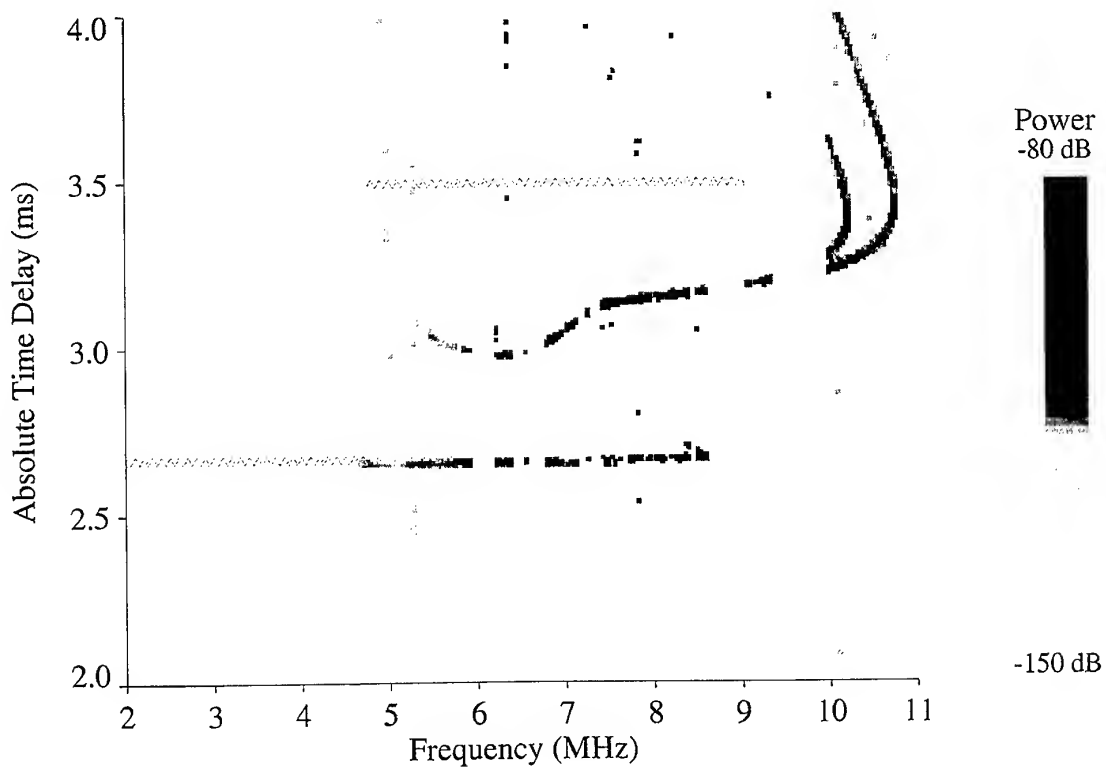


Figure 6-13: IRIS ionogram recorded on the Lancaster-Saxa Vord path at 15:16UT on 6th April 1994. Green triangles represent predictions of the ITU Rec. 533 model.

7 Conclusions

- 7.1 A state-of-the-art analytical ray tracing technique called SMART (Segmented Method for Analytical Ray Tracing) has been compared with a highly accurate but slow numerical ray tracing procedure and also with a simple 'virtual mirror' semi-empirical technique (ITU Rec. 533) which determines ground range as a function of elevation angle. Results indicate a close agreement between analytical and numerical ray tracing ground range predictions whilst the virtual mirror technique can be greatly in error, particularly in the transition regions between E and F modes of propagation.
- 7.2 A homing algorithm has been developed in conjunction with the SMART ray-tracing algorithm to rapidly home a ray to a particular ground range. This may be implemented over a range of transmission frequencies to produce a synthesised oblique incidence (OI) ionogram.
- 7.3 Validation of the accuracy of the ionospheric electron density models PIM, FAIM, IRI-95 and PRISM has been performed by comparison of synthetic OI ionograms with measured OI ionograms recorded on six UK paths. OI ionograms were also synthesised from the ITU Rec.533 model and compared with the measured OI ionograms.
- 7.4 Synthetic OI ionograms produced by ray tracing through either the tomographic images or the climatological models showed that on average, the maximum usable frequency (MUF) of the E trace (MUF(E)) was underestimated by both the tomography and the best climatological model (IRI-95). The latter underestimated MUF(E) by only 1.4% compared with at least 5.3% for the best tomographic method.
- 7.5 In contrast tomography generally overestimated MUF(F2); however in this case tomography performed better than the climatological models. The best tomographic method predicted a mean 0.8% overestimate compared with 3.3% for the best climatological method. Climatology also showed larger rms errors than tomography for both MUF(E) and MUF(F2), probably due to their inability to model real-time fluctuations in the ionosphere.
- 7.6 When no ionosonde was used to provide *a priori* information in the tomographic reconstruction, the average underestimate of MUF(E) increased from 5.3% to 20.2% and the average MUF(F2) overestimate increased from 0.8% to 3.3%. In our tests the use of more than one ionosonde did not reduce further the errors associated with the tomographic images. We recommend, therefore, that a single ionosonde should be used in conjunction with the tomographic receiver chain.
- 7.7 The minimum delay of the E trace ($m'd(E)$) (a measure of the height of the E layer) was better represented by tomography (0.1% mean underestimate) than climatology (at least 2.1% mean error). However, tomography consistently underestimated the minimum delay of the F trace (by at least 2.8%) unlike the climatological models (mean underestimate 0.5%).
- 7.8 Tomography, unlike the climatological models, consistently underestimated the minimum delay of the F trace.

8 Recommendations for Further Work

8.1 Validation and Development of the PRISM model

- 8.1.1 It is important that PRISM be validated for a wide range of ionospheric conditions. This is hard enough at mid latitudes where there is little structure but it is particularly difficult at high latitudes. DERA now have available a database of over 1000 tomographic images. These images were recorded over the UK between Oct 1997 and April 1999 and measurements from the vertical ionosonde at Chilton were incorporated into the reconstruction of the images. We recommend that PRISM be compared with the tomographic images at geographic latitudes of 45-65°N, to identify errors, particularly in the latitudinal structure of the ionosphere and the location of large-scale ionospheric structures such as the sub-auroral trough.
- 8.1.2 It had been hoped that this could have been pursued within this contract but PRISM was not made available until the end and only limited analysis could be carried out. In particular any comparisons should be carried out in conjunction with ray tracing since it is important to understand the systems impact of any modelling errors. Such ray tracing should focus on both HF and trans-ionospheric systems.
- 8.1.3 As an example, predictions of slant-TEC from the PRISM (or any other) model could be compared directly with TEC measurements from the individual UK tomographic receivers. This would determine the accuracy of the ionospheric model as applied to trans-ionospheric propagation (e.g. for correcting ionospheric errors on satellite navigation systems).

8.2 Importance of the F1 layer

- 8.2.1 Most ionospheric models fail to include real-time parameters of the F1 region (e.g. from ionogram traces). This leads to large errors in the predictions of group delay of reflections from the F region when the F1 layer is present. This can in turn lead to large errors in the calculation of ground range.
- 8.2.2 The incorporation of F1 parameters (or a full profile of electron density determined from vertical ionograms) should be a priority in the development of real-time ionospheric models used in connection with HF ray tracing algorithms.

9 Acknowledgements

- 9.1 The authors gratefully acknowledge the US Air Force Research Laboratory, Hanscom AFB, MA, Computational Physics, Inc. (Boston Office) Norwood, MA, and Headquarters of US Air Force Space Command (HQ AFSPC) for providing the ionospheric models FAIM, PIM and PRISM used in this research.
- 9.2 The IRI-95 model was provided by the US National Space Science Data Center (NSSDC).
- 9.3 The authors are particularly grateful for Drs Kent Millar (EOARD), Paul Kossey and Terence Bullett (AFRL) for their interest and help in this project.

10 References

- Anderson, D.N., M. Mendillo and B. Herniter, "A Semi-Empirical, Low-Latitude Ionospheric Model", *Radio Science* 22, 292, 1987.
- Anderson, D.N., J.M. Forbes and M. Codrescu, "A Fully Analytical, Low- and Middle-Latitude Ionospheric Model", *J. Geophys. Res.* 94, 1520, 1989.
- Arthur, P C, M Lissimore, P S Cannon and N C Davies, "Application of a High Quality Ionosonde to Ionospheric Research", *IEE 7th International Conference on HF Radio Systems and Techniques*, Conf. Publ. 441, 135, Nottingham, July 1997.
- Bilitza, D., N. M. Sheikh, and R. Eyfrig, "A Global Model for the Height of the F2-Peak Using M(3000)F2 Values from the ITU Numerical Map", *Telecomm. J.*, 46, 549, 1979.
- Bilitza, D. (ed.), *International Reference Ionosphere 1990*, NSSDC 90-22, Greenbelt, Maryland, 1990.
- Booker, H.G., "Fitting of multi-region ionospheric profiles of electron density by a single analytic function of height", *J. Atmos. Terr. Phys.*, 39, 619-623, 1979.
- Bradley P.A. and J.R. Dudeney, "A Simple Model of the Vertical Distribution of the Electron Density of the Electron Concentration in the Ionosphere", *J. Atmos. Terr. Phys.*, 35, 2131-2146, 1973.
- Budden, K.G., "Radio Waves in the Ionosphere", Cambridge University Press, Cambridge, 1961.
- ITU Recommendation 533-3 - "CCIR HF Propagation Prediction Method" (1978-1982-1990-1992) pp57-71 International Telecommunication Union CCIR Recommendations, RPI Series 'Propagation in Ionised Media', Geneva, 1992.
- Chiu, Y.T. "An Improved Phenomenological Model of Ionospheric Density", *J. Atmos. Terr. Phys.* 37, 1563, 1975.
- Croft, T.A. and H. Hoogasian, "Exact ray calculations in a quasi-parabolic ionosphere", *Radio Sci.* 3, 69-74, 1968.
- Daniell, R.E. Jr., "Parameterised real-time ionospheric specification model. PRISM Version 1.0", Phillips Lab. Tech. Rep. PL-TR-91-2299, December 1991.
- Daniell, R.E. Jr., L.D. Brown, D.N. Anderson, M.W. Fox, P.H. Doherty, D.T. Decker, J.J. Sojka and R.W. Schunk, "PIM: A Global Ionospheric Parameterization Based on First Principles Models", *Radio Sci.* 30, 1499-1510, 1995.
- Dudeney, J.R. *Brit. Antarctic Surv. Sci. Rept.* 88., 1974.
- Dudeney, J.R., "An Improved Model of the Electron Concentration with height in the Ionosphere", *J. Atmos. Terr. Phys.* 40, 195-203, 1978.
- Folkestad, K., "Exact ray calculations in a tilted ionosphere with no magnetic field.", *Radio Sci.*, 3, pp81-84, 1968.
- Haselgrove, J. "Ray theory and a new method for ray-tracing." Report on the conf. on the physics of the ionosphere, Cambridge, 1954, (Physical Society, London), *Proc. Phys. Soc. London*, 23, pp355-364, 1955.
- Hedin, A. E., "MSIS 86 Thermospheric Model", *J. Geophys. Res.*, 92, 4649-4662, 1987.
- Jones, R.M., "Three-dimensional ray-tracing computer program", *Radio Sci.* 3, pp93-94, 1968.
- Jones R.M. and J.J. Stephenson, "A versatile three-dimensional ray tracing computer program for radio waves in the ionosphere", Rep. 75-76, Office of Telecommunications, Boulder, Colorado, 1975.
- Norman, R.J., J.A. Bennett, P.L. Dyson and L. Nguyen, "HIRT Homing-In Ray Tracing", Research Report, School of Physics, La Trobe University, 1994.
- Norman, R.J., I.G. Platt and P.S. Cannon, "An analytic ray tracing model for HF ionospheric Propagation", 4th AGARD symposium on digital communications systems: propagation effects, technical solutions, systems design, Athens, Greece, September, 1995.
- Norman, R.J. and P.S. Cannon, "A two-dimensional analytical ray tracing technique accommodating horizontal gradients", *Radio Sci.* 32, (2), pp387-396, 1997.
- Norman, R.J. and P.S. Cannon, "An evaluation of a new 2D analytic ionospheric ray tracing technique - SMART", *Radio Sci.*, 33, 1999.

- Platt, I.G. and P.S. Cannon, "A propagation model for the mid and high latitude ionosphere over Europe", IEE Conf. Publ. 392, 86-90, 1994.
- Rawer, K., "International Reference Ionosphere - IRI 79", Rep. UAG-82, 243 pp., Natl. Oceanic and Atmos Admin., Washington, D.C., 1981.
- Rawer, K. et al. (eds) Adv. Space Res. 16, (1), 1995
- Rawer, K. et al. (eds) Adv. Space Res. 18, (6), 1996
- Rogers, N.C. "SMART Version 1.0: An analytical ray tracing computer program", DERA Software User Manual, DERA/CIS/CIS1/SUM980487, 1998.
- Rogers, N.C., P.S. Cannon, J.A.T. Heaton, C.N. Mitchell and L. Kersley, "Ray tracing through tomographic images of the ionosphere", IEE National Conference on Antennas and Propagation, 31 March – 1 April, University of York, York, UK, IEE Publ. No. 461, 345-348, 1999.
- Schunk, R.W., "A mathematical model of the middle and high latitude ionosphere." Pageoph., 127, pp255-303, 1988.
- Shukla, A.K., P.S. Cannon, S. Roberts, and D. Lynch, "A tactical HF decision aid for inexperienced operators and automated HF systems", IEE Conf. Publ. 441, p383-387, 7th International Conference on HF Radio Systems and Techniques, East Midlands Conference Centre, Nottingham, UK, 7-10 July 1997.

Reference is also made to the following unpublished material:-

- Rogers, N.C., A. Akram and P.S. Cannon, "A Comparison of Analytical, Numerical and Virtual Mirror, HF, Ray tracing Methods", DERA technical report (unpublished), February 1998.

11 List of Symbols

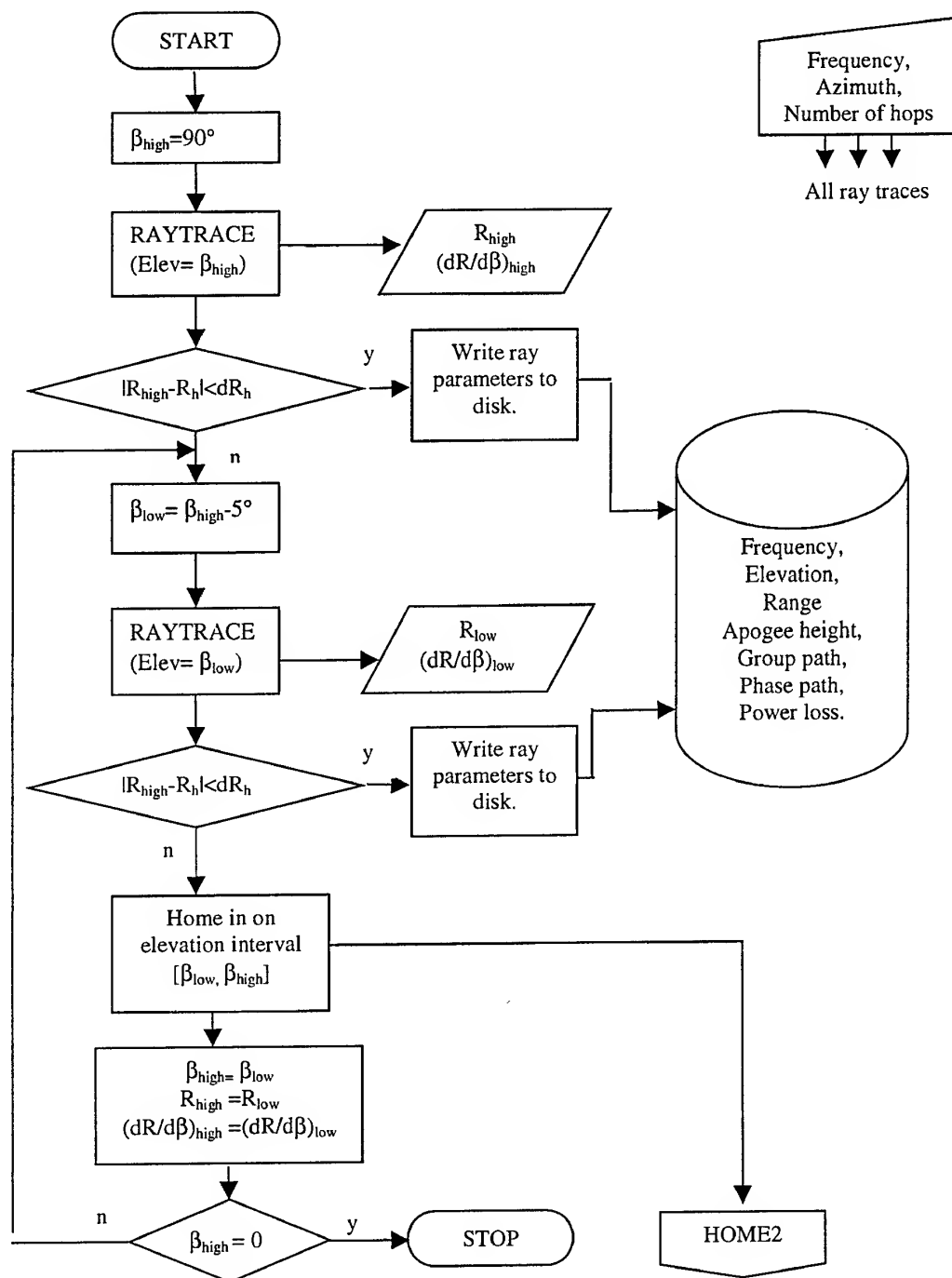
β_o	Launch elevation angle
B_y	Dawn-dusk component of the interplanetary magnetic field
B_z	Northward component of the interplanetary magnetic field
c	Speed of electromagnetic waves in free space
$dR/d\beta$	Rate of change of ground range with launch elevation angle
dR_h	+/- Tolerance on homing range
foE	(see foF2)
$foF1$	(see foF1)
$foF2$	Plasma frequency at peak of ionospheric F2 region. (i.e. the minimum (HF) frequency of an o-ray that, propagated vertically, does not penetrate the ionosphere)
$h'E$	virtual height of radiowave reflection in the E region
$h'F1$	virtual height of radiowave reflection in the F1 region
$h'F(F2)$	virtual height of radiowave reflection in the F (or F2) region
h_mF2	height of maximum electron density in the F2 region
K_p	(a planetary geomagnetic activity index)
$M(3000)F2$	$= MUF(3000)/foF2$. A propagation factor closely related to the height of the F2-peak (see <i>Bilitza et al.</i> , [1979])
$m'd(E)$	minimum delay of the E trace on ionograms
$m'd(F1)$	minimum delay of the F (or F1) trace on ionograms
$m'd(F(F1))$	minimum delay of the F (or F1) trace on ionograms
$m'd(F2)$	minimum delay of the F2 trace on ionograms
$MUF(3000)$	the highest frequency that, refracted in the ionosphere, can be received at a distance of 3000 km
R	Ground range
R_{12}	Zurich 12-month smoothed sunspot number
R_h	Homing-in ground range
R_{high}	Ground range of ray at high elevation angle
R_{low}	Ground range of ray at low elevation angle
y_mF2	Semi-thickness of the F2 layer

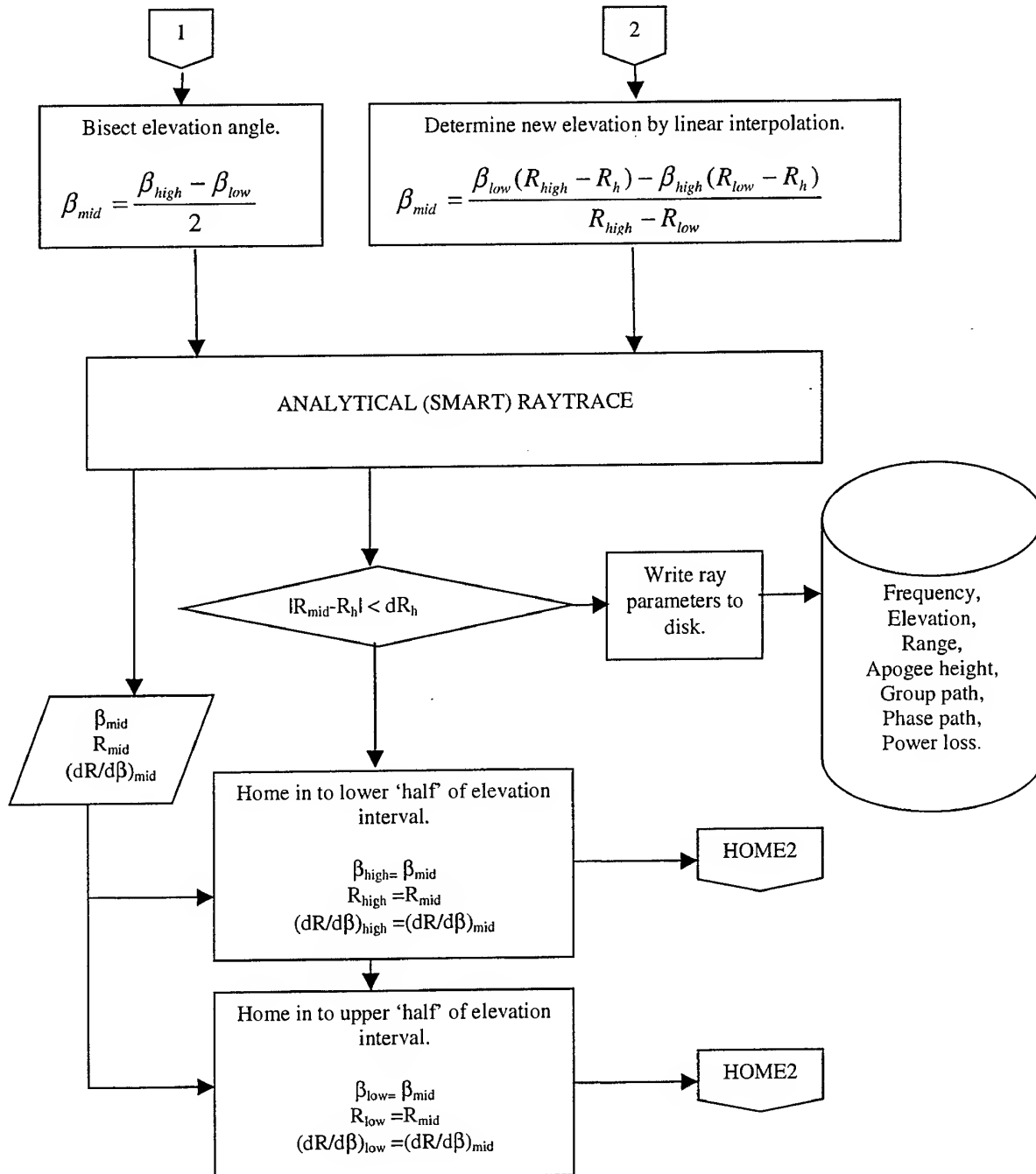
12 List of abbreviations

AFRL	(US) Air Force Research Laboratories
C ³ I	Command, Communication, Control and Intelligence
CCIR	International Radio Consultative Committee
CT	Computerised Tomography
DERA	Defence Evaluation and Research Agency
DF	Direction Finding
DUD	Dudeney model electron density profile [<i>Dudeney</i> , 1978]
EDP	Electron density profile
EEMS	Electromagnetic Environmental Management System
EOARD	(US) European Office for Aerospace Research and Development
FAIM	Fully Analytical Ionospheric Model
GPS	Global Positioning (Satellite) System
HF	High Frequency (3-30MHz)
HIRT	Homing-In Ray Tracing (a numerical ray tracing program)
IRIS	Improved Radio Ionospheric Sounder
ITU	International Telecommunications Union
MoD	Ministry of Defence (UK)
MQPS	Multi-quasi-parabolic segments
MSIS	Mass Spectrometer - Incoherent Scatter (upper atmosphere model)
MUF(E)	Maximum Usable Frequency of the E, o-ray trace
MUF(F)	Maximum Usable Frequency of the F o-ray trace
NIMS	Naval Ionospheric Monitoring System
NODECA	Office for the Norwegian Defence Telephone and Data Services
OI	Oblique Incidence
o-ray	Ordinary ray (not subject to magneto-ionic splitting)
PIM	Parameterised Ionospheric Model
PRISM	Parameterised Real-time Ionospheric Specification Model
QP	Quasi-parabolic
QPS	Quasi-Parabolic Segment
RAL	Rutherford-Appleton Laboratory
rms	Root-mean-square
SATCOM	Satellite Communications
SLIM	Semi-Empirical, Low-latitude Ionospheric Model
SMART	Segmented Method for Analytical Ray Tracing
SSN	Sunspot number
TEC	Total Electron Content (the line integral of the electron density)
UHF	Ultra-High Frequency (300MHz-3GHz)
UK	United Kingdom (of Great Britain and Northern Ireland)
US	United States (of America)
VHF	Very High Frequency (30-300MHz)
VI	Vertical Incidence

A Flow diagram for homing ray trace algorithm

- A.1 The following pages provide a flowchart description of the homing algorithm developed in conjunction with the analytical ray tracing code for the synthesis of oblique ionograms. The homing technique is also explained in Section 5 of the main report.
- A.2 The symbols used in the flowchart are defined in Table 6 (page 20).





Distribution list

Name	Organisation	Copy Number
Prof. P.A. Watson	University of Bath, UK	1-10

This page is intentionally blank

REPORT DOCUMENTATION PAGE

Form Approved OMB No. 0704-0188

Public reporting burden for this collection of information is estimated to average 1 hour per response, including the time for reviewing instructions, searching existing data sources, gathering and maintaining the data needed, and completing and reviewing the collection of information. Send comments regarding this burden estimate or any other aspect of this collection of information, including suggestions for reducing this burden to Washington Headquarters Services, Directorate for Information Operations and Reports, 1215 Jefferson Davis Highway, Suite 1204, Arlington, VA 22202-4302, and to the Office of Management and Budget, Paperwork Reduction Project (0704-0188), Washington, DC 20503.

1. AGENCY USE ONLY (Leave blank)		2. REPORT DATE November 1999		3. REPORT TYPE AND DATES COVERED Final; November 1999	
4. TITLE AND SUBTITLE Evaluation of Modern HF Ray Tracing (Final Report)				5. FUNDING NUMBERS F61775-98-WE133 CSM 7153 FY98/99	
6. AUTHOR(S) Neil Rogers					
7. PERFORMING ORGANIZATION NAME(S) AND ADDRESS(ES) DERA Malvern St. Andrews Rd. Malvern, Worcester, WR14 3PS United Kingdom				8. PERFORMING ORGANIZATION REPORT NUMBER DERA/CIS/CIS1/CR990854	
9. SPONSORING/MONITORING AGENCY NAME(S) AND ADDRESS(ES) EOARD PSC 802 Box 14 FPO 09499-0200				10. SPONSORING/MONITORING AGENCY REPORT NUMBER SPC 98-4091	
11. SUPPLEMENTARY NOTES This report downgraded from "US For Official Use Only" to "Unlimited", 17 May 2001.					
12a. DISTRIBUTION/AVAILABILITY STATEMENT Approved for Public Release; Distribution Unlimited Crown copyright 1999 DERA; U.S. Government Purpose Rights				12b. DISTRIBUTION CODE A	
12. ABSTRACT (Maximum 200 words) This report results from a contract tasking Department of Electronic and Electrical Engineering, University of Bath, Claverton Down, Bath BA2 7AY, UK, as follows: The contractor will investigate the accuracy and improved performance in determining HF propagation by coupling a state-of-the-art ray tracing technique with a physics-based ionospheric model. The accuracy of a novel segmented method for analytic ray tracing (SMART) developed at DERA is reported alongside numerical and virtual mirror ray tracing techniques. A description is given of homing technique for the synthesis of oblique incidence (OI) ionograms by means of SMART ray tracing. Synthetic OI ionograms have been compared against measured OI ionograms on six UK paths. By scaling key parameters from each ionogram (synthetic vs. measured) the accuracies of four climatological ionospheric models, tomographic images and the parameterised Real-time Ionospheric Specification Model (PRISM) are described.					
14. SUBJECT TERMS EOARD, Space Science, Communications, Radio propagation, Ionosphere, HF, PRISM				15. NUMBER OF PAGES	
				16. PRICE CODE	
17. SECURITY CLASSIFICATION OF REPORT UNCLASSIFIED	18. SECURITY CLASSIFICATION OF THIS PAGE UNCLASSIFIED	19. SECURITY CLASSIFICATION OF ABSTRACT UNCLASSIFIED	20. LIMITATION OF ABSTRACT UL		

NSN 7540-01-280-5500

Standard Form 298 (Rev. 2-89)
Prescribed by ANSI Std. Z39-18
298-102

Prof. Paul Cannon
Dept of Electrical and Electronic Engineering,
University of Bath,
Bath,
UK.

Dr. Neil Rogers
D714, DERA Malvern
St. Andrews Road, Malvern
Worcestershire, WR14 3PS
United Kingdom

Tel: +44 (0)1684 896141
Fax: +44 (0)1684 895241
Email: nerogers@dera.gov.uk

Our Reference:
Your Reference:

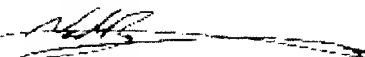
17 May 2001

Dear Paul,

Acting on behalf of Prof. Peter Watson as customer and recipient of report DERA/CIS/CIS1/CR990854 you recently requested my authority to downgrade its protective marking from "UK UNCLASSIFIED - US FOR OFFICIAL USE ONLY" to "UNLIMITED". As the originator of the report I have authorised this change by completing and returning the MOD form 171 (enclosed). I will send a copy of this form, together with a copy of this letter to the DERA Defence Research Information Centre (DRIC).

Please remark all copies of the report in your possession accordingly, and inform all known recipients of the report to do likewise.

Yours sincerely,



Neil Rogers

Enc.: completed MOD form 171

cc: Karen Jackson-Morris. DERA-DRIC, Glasgow.

Part 1 - request for downgrading of protectively marked documents

To: DR. NEIL ROGERS DTIC DERA MALVERN ST. ANDREWS RD, MALVERN, WORCS WR14 3PS	From: PROF. PAUL CANNON DEPT. ELECTRICAL & ELECTRONIC ENGINEERING UNIVERSITY OF BATH, UK
---	---

It is requested that authority be given for the downgrading of the documents listed overleaf.
 If downgrading is agreed, please state new protective marking in column (e); otherwise insert "No change".

Date...17/5/01.....

Signature.....

Reverse


Part 2 - authority to downgrade protectively marked documents

To: PROF. PAUL CANNON UNIVERSITY OF BATH	From: NEIL ROGERS DERA MALVERN
--	--

Please note that the documents listed below should now be graded as shown in column (e)

Reference No. (a)	Description (i.e. File, letter, report etc.) (b)	Date (c)	Present protective marking (d)	Revised protective marking (e)
DERA/CIS/CIS/CR990854	REPORT	NOV 1999	UK UNCLASSIFIED - US FNM OFFICIAL USE ONLY	UNLIMITED
_____	_____	_____	_____	_____
_____	_____	_____	_____	_____

Date...17/5/01.....

Signature.....

Grade...SSO (LEVEL 5)